Fluvial reworking eliminates small craters, but does not meaningfully bias the Mars interbedded-crater record

Andrew J. Moodie[1,2], **Timothy A. Goudge**[2,3]

[1]Department of Geography, Texas A&M University
[2]Department of Earth and Planetary Sciences, Jackson School of Geosciences, The University of Texas at Austin
[3]Center for Planetary Systems Habitability, The University of Texas at Austin

Key Points:

- We simulated coeval river-delta and crater production, and quantified crater preservation in resulting fluvial-deltaic stratigraphy
- Our findings indicate smaller craters are more often removed by fluvial reworking than larger craters
- More smaller craters are produced than rivers can remove, bolstering some interpretations of atmospheric paleo-pressure

THIS IS PREPRINT OF A RESEARCH ARTICLE SUBMITTED TO *Journal of Geophysical Research: Planets* ON 04/26/24. IT HAS NOT COMPLETED PEER REVIEW, AND HAS NOT BEEN ACCEPTED FOR PUBLICATION.

Corresponding author: Andrew J. Moodie, amoodie@tamu.edu

Abstract

Interpreting the structures, morphology, and chemistry of the exposed stratigraphic record on Mars is complicated by ancient surface processes that have variably removed parts of the record. Previous research has used the lack of smaller craters ($\leq$50 m diameter) interbedded with fluvial deposits to constrain atmospheric pressure when rivers were active on Mars; the notion being that higher atmospheric pressure would have prevented smaller craters from forming. We hypothesize that contemporaneous channel lateral migration and avulsion could have reworked sedimentary deposits and eliminated craters from the stratigraphic record, thereby undermining atmospheric paleo-pressure interpretations. To test this hypothesis, we simulated coeval river-delta development and crater production, and quantified crater preservation in resulting stratigraphy. We document widespread crater rim degradation ($\sim$67% of craters $\leq$50 m are at least partially eroded), and observe a marked increase in preservation with increasing crater diameter. That is to say, fluvial reworking preferentially removes smaller craters from the stratigraphic record. However, synthetic crater-diameter distributions incorporating fluvial reworking effects do not reproduce observations on Mars, because many smaller craters generated remain preserved in the simulated stratigraphy. We find that, although river channels are sometimes in the right place to eliminate crater deposits from the stratigraphic record, production of smaller craters outpaces fluvial reworking under all modeled circumstances, and that a higher pressure ancient atmosphere is necessary to reproduce observations (i.e., consistent with existing interpretations of interbedded crater records). Our findings therefore bolster studies that assert fluvial reworking is not a primary control on smaller interbedded crater counts on Mars.

Plain Language Summary

Higher atmospheric pressure causes small impactors to break up before reaching the ground. So, researchers have used the lack of small craters observed from a specific time interval on Mars to infer what the atmospheric pressure was during that time interval. This has been particularly useful for early Mars, when water was thought to have been more abundant, implying the need for a thicker atmosphere. We hypothesized that another process, rivers migrating across the landscape, could preferentially remove small craters from the observable record, and had misled researchers into thinking the lack of craters was due to high atmospheric pressure on ancient Mars. We tested our hypothesis with numerical modeling, and found that while migrating rivers can remove craters from the record, this process cannot remove enough craters to explain the complete lack of small craters on Mars.

1 Introduction

Decades of research have leveraged the sedimentary structures, morphology, and chemistry of the exposed stratigraphic record on Mars to understand the evolution of the planet's ancient surface and atmosphere (e.g., Cabrol et al., 1999; Malin & Edgett, 2000; J. Grotzinger et al., 2005; Milliken et al., 2010; J. P. Grotzinger et al., 2012-09; Cardenas et al., 2017; Goudge et al., 2018; Bishop et al., 2018; Day et al., 2019; Cardenas & Lamb, 2022; Vasavada, 2022). Of particular interest, is the formation timing of alluvial and lacustrine features on Mars, because these features likely demarcate the extent and duration of past hydrological activity that could have enabled life on the planet's surface (e.g., Bhattacharya, 2005). Without any direct sample dating as of the time of writing, absolute temporal constraints on formation of these features are determined by measured crater size-frequency distributions (CSFDs) that are paired with expected crater production rate models (i.e., crater counting; Hartmann, 1966; Hartmann & Neukum, 2001; Ivanov, 2001; Fassett, 2016). Interpreting crater records, and in particular those records from a planet with active sedimentary

surface processes, is complicated by the interplay of ancient and modern surface processes that create, eliminate, and expose stratigraphic features (Jerolmack & Sadler, 2007; Kim et al., 2014; Cardenas et al., 2022). For example, it is well known that modern surface processes can readily degrade smaller craters ($\lesssim$50 m) to the point the crater is unrecognizable (e.g., Hartmann, 1971; Fassett, 2016; Williams et al., 2018), and therefore bias the observed crater record. There remains considerable uncertainty in how and under what circumstances the Mars crater record is biased by surface processes (Williams et al., 2018), and what the impact of this bias is on sedimentary feature age estimates (M. Golombek et al., 2010).

The lack of smaller craters ($\lesssim$50 m) embedded in the Mars stratigraphic record that is now exposed at the surface, has been used to constrain atmospheric paleo-pressure (e.g., Figure 1a; Kite et al., 2014; Warren et al., 2019). These studies determine atmospheric pressure from crater sizes by assuming a relationship between atmospheric pressure and the smallest size of impactors that can reach the planet surface before complete ablation (e.g., higher atmospheric pressure raises the lower limit of possible crater size; Popova et al., 2003; Williams et al., 2014). The additional assumption that atmospheric ablation is the only significant process impacting crater size distributions, enables an inversion from the measured CSFDs to atmospheric paleo-pressure, yielding an upper-bound pressure, in essence, based on the *lack* of smaller craters. Kite et al. (2014) isolated craters interbedded with fluvial deposits and that therefore formed when Mars rivers were active, and determined that the Mars atmosphere would have been less than $\sim$1.9 bar approximately 3.5 Ga. In another study using a similar approach, Warren et al. (2019) found that Mars paleo-pressure was approximately 1.5 and 1.9 bar at 3.8 and 4 Ga, respectively (or oscillated around these values; Warren et al., 2019).

Atmospheric paleo-pressure interpretations are especially sensitive to identification of smaller craters ($\lesssim$50 m). Prior studies have examined preferential destruction of smaller craters due to wind-blown erosion (Öpik, 1966; Hartmann & Neukum, 2001), diffusive down-slope transport driven by subsequent impacts (Ross, 1968; Soderblom, 1970; A. Howard, 2004; Minton et al., 2015), and flattening by seismic-shaking (Schultz & Gault, 1975; Richardson et al., 2004, 2005), as well as covering by lava flows (Neukum & Horn, 1976; Hiesinger et al., 2002; Michael, 2013), and obliteration during formation of new craters (i.e., saturation; Woronow, 1977, 1978; M. R. Smith et al., 2008; Richardson, 2009; Minton et al., 2015). Other studies have discussed the potential for erosion by fluvial processes to remove smaller craters (Irwin et al., 2013; Matsubara et al., 2018), but this has not been examined in the context of craters that could become interbedded in a fluvial sedimentary deposit (e.g., those craters in Kite et al., 2014). The potential impact of smaller crater removal on paleo-pressure interpretations has not been rigorously evaluated.

River and delta activity is spatially and temporally heterogeneous, due to the movement of channels across the landscape over time (Schumm, 1985; Straub et al., 2009). This channel movement causes local fluctuations in deposition and erosion that create a stratigraphic record rife with gaps and bias in recorded time (Sadler, 1981; Hajek & Straub, 2017; Straub et al., 2020). For example, individual channel bends translate across the landscape eroding deposited material (e.g., Schumm, 1985), and leaving behind characteristic lateral accretion deposits, that are commensurate in height to the channel depth (e.g., Figure 1b; Edwards & Eri, 1983; Bridge & Mackey, 1992). At larger space and time scales, channels regularly relocate across the floodplain via avulsion, wherein flow is steered across the landscape surface by topography and a new channel pathway is developed (e.g., Frazier, 1967; Wells & Dorr, 1987; N. D. Smith et al., 1989; Hajek & Edmonds, 2014).

As a result of these channel movements, fluvial reworking of stratigraphy is scaled to a first order by channel depth and channel mobility (Leeder, 1978; Ganti et al., 2011; Straub & Esposito,

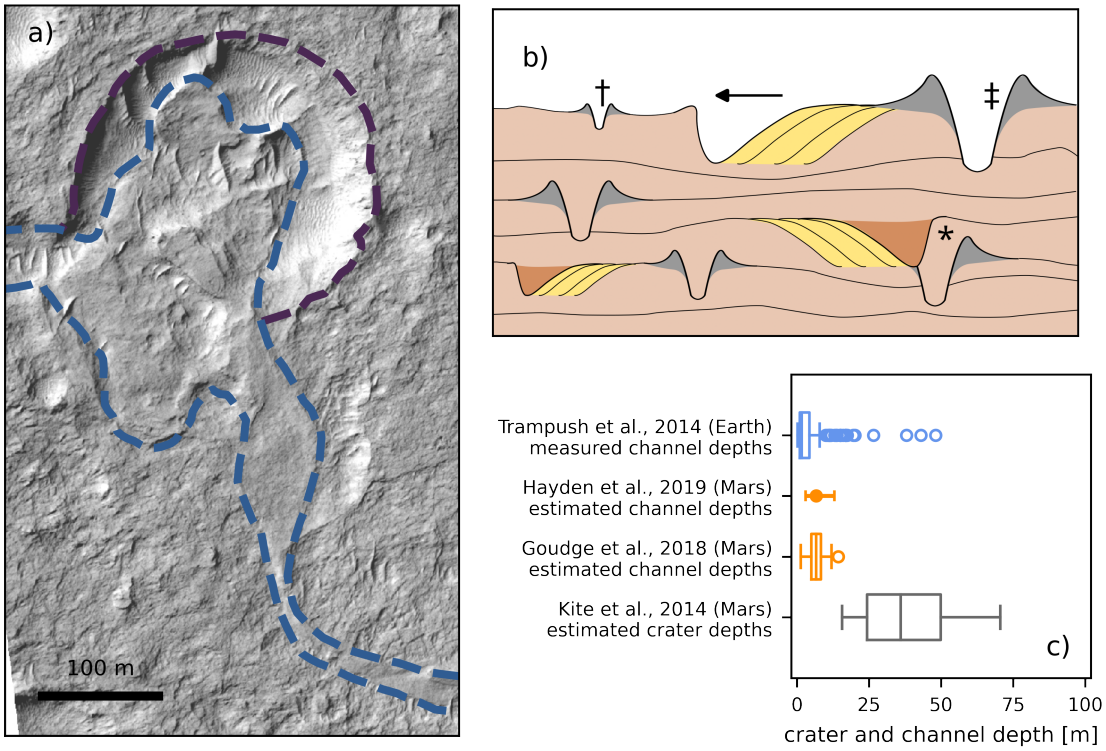

Figure 1. a) Example of a 238 m diameter crater (purple dashed line) interbedded with fluvial deposits (blue dashed lines) identified by Kite et al. (2013). Crater is located in the Aeolis Dorsa region, Mars (153.803E, 5.991S; HiRISE image ESP_017548_1740; NASA/JPL-Caltech/UArizona; McEwen et al., 2007). b) Schematic cross-section of channel and crater interactions in the production of stratigraphy. The ← marks the migration direction of a channel located at the surface, which was steered by a larger crater rim marked by the ‡. The † indicates a crater rim that may be removed from the record due to ongoing channel migration and the relative size of the channel and crater rim. In contrast, the larger crater rim (‡) is unlikely to be removed, due to its position relative to the migration direction and larger size. In the stratigraphy, there are several fully preserved channel lateral migration deposits, and a crater rim that is partially preserved (marked by *), due to erosion by a migrating channel. c) Channel and crater depths on Earth and Mars (Trampush et al., 2014; Goudge et al., 2018; Hayden et al., 2019) have similar absolute scales to depths of craters missing from the ancient stratigraphic record on Mars, which has been used to estimate paleo-atmospheric pressure (Kite et al., 2014); here, a boxplot characterizes a distribution, and the solid circle and bar indicates a mean and range.

2013; Wickert et al., 2013; Straub et al., 2015; Hajek & Straub, 2017). For example, a deeper channel reaches farther into the subsurface and erodes sediment over a larger cross-sectional area, and a more rapidly migrating or avulsing channel increases the proportion of the landscape visited and where stratigraphy is destroyed. Moreover, whether a fluvial system is dominated by channel migration or avulsion is also known to affect stratigraphic reworking (Straub et al., 2009; Wang et al., 2011), with dominance between the two mobility modes being related to, among other factors, sediment composition (Straub et al., 2015; Liang et al., 2015a, 2016; Hajek & Straub, 2017). Finally, the fluvial system aggradation rate also affects stratigraphic reworking, because slower aggradation keeps sediments near the surface and within reach of channels for an increased duration (Hajek & Straub, 2017).

Coincidentally, typical river channel depths have similar absolute scales to smaller crater depths (Figure 1b,c). For example, typical alluvial river channel depths range 1–5 m on Earth (Trampush et al., 2014) and are estimated to have been 2–10 m on Mars (Goudge et al., 2018; Hayden et al., 2019), and crater depths range <1–20 m for craters $\lesssim$50 m in diameter. Notably, initial crater depths of craters measured by Kite et al. (2014) would have been mostly deeper than estimated channel depths (Figure 1c), opening the possibility that the "missing" smaller craters were removed from the record by migrating river channels, and therefore not observed when strata were later exhumed and interbedded crater sizes were mapped (Kite et al., 2014). Moreover, it is known that ancient channels moved across the Mars landscape when the stratigraphic interval of interest was produced (Goudge et al., 2018; Hayden et al., 2019; Cardenas & Lamb, 2022).

Overlapping absolute dimensions of fluvial channels and smaller craters raise the possibility that fluvial reworking has removed a substantial portion of smaller interbedded craters from the Mars stratigraphic record. Indeed, if fluvial reworking substantially biased the Mars crater record, the lack of smaller craters would not be a robust proxy for atmospheric paleo-pressure (Kite et al., 2014). Warren et al. (2019) applied an analytical size-dependent filter to approximate crater removal by sedimentary processes and investigate if these processes could meaningfully change paleo-pressure interpretations. Their study determined that the process-filter could not explain the observed Mars crater record, but the functional form and parameterization of the analytical filter were not calibrated or validated. We hypothesize that fluvial activity can rework and eliminate from the stratigraphic record crater deposits that form proximally to river channels (i.e., interbedded craters).

We further hypothesize that because smaller craters ($\lesssim$50 m diameter) present a less significant physical obstacle to a laterally migrating or avulsing river than larger craters ($\sim$50–300 m diameter), there is a crater size-dependent bias in the removal of craters by fluvial reworking. This preferential removal of smaller craters would adjust atmospheric paleo-pressure interpretations downwards, by confirming the possibility that unobserved crater diameters were eliminated by fluvial reworking, rather than by atmospheric ablation.

In this study, we answer the question: can fluvial reworking explain the lack of smaller interbedded craters ($\lesssim$50 m) on Mars? We first forward modelled coeval river-delta evolution and crater production, and assessed preservation of craters within the fluvial-deltaic stratigraphy. With these observations, we studied how crater size-frequency distributions are impacted by fluvial reworking, and determine how to account for this bias when making atmospheric paleo-pressure interpretations.

2 Modeling crater production and delta sedimentation

We simulated river-delta development with coeval crater production using open-source research software. We use Python 3.9.5 and *pyDeltaRCM* v2.1.4 for delta modeling (Moodie et al., 2021), and coupled it with crater size-frequency distributions generated with *craterstats2* v3.0.11 (Michael et al., 2016), and an analytical framework describing fresh crater geometries (A. D. Howard, 2007). Our workflow is fully reproducible, and all modeling and analysis codes are archived, with links to repositories in the Open Research Section.

2.1 Crater size-frequency distributions

The accumulated history of crater production and destruction is recorded in crater size-frequency distributions (CSFDs). Most commonly, a crater size-frequency distribution (CSFD) is measured over a control area and used to constrain surface age (e.g., Fassett, 2016). This approach com-

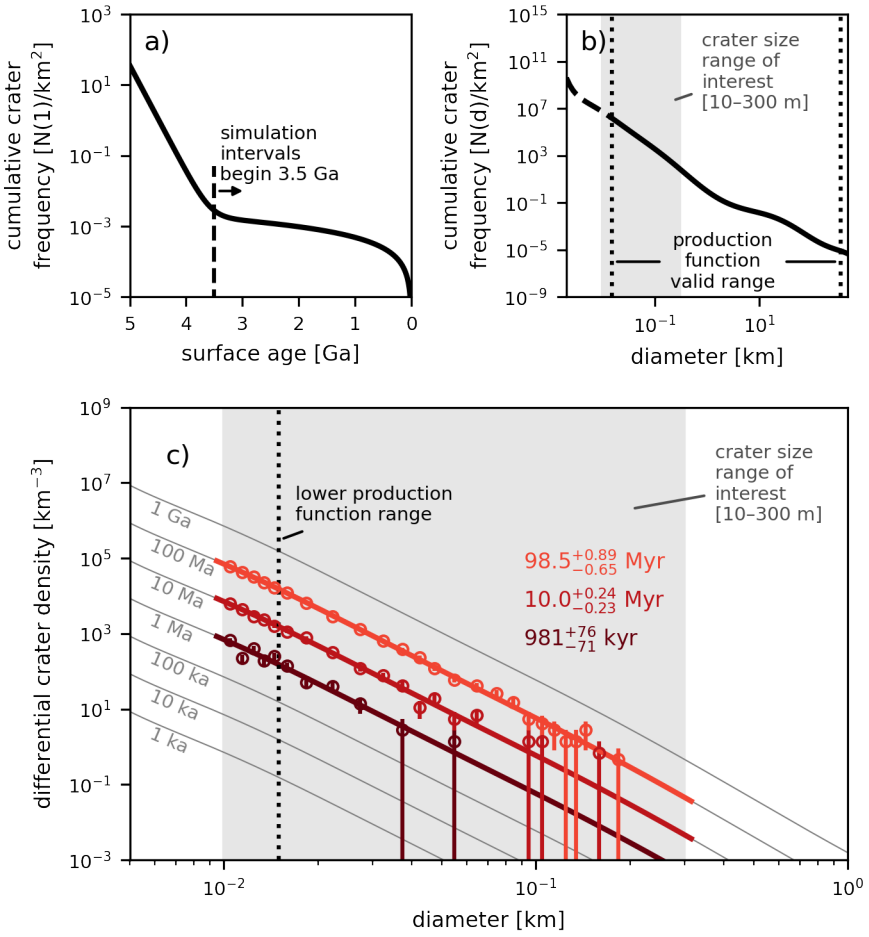

Figure 2. a) The Hartmann and Neukum (2001) Mars chronology function, describing the number of 1 km diameter craters per km^2, accumulated on a surface with a given age. b) The Ivanov (2001) Mars production function, describing the relative abundance of craters by diameter. c) The chronology function and production function are used together in a Monte Carlo simulation to generate crater-size populations representing time durations of 1 Ma, 10 Ma, and 100 Ma, and beginning 3.5 Ga, which are then used in model simulations (see text for additional details; Michael et al., 2016).

pares the measured CSFD to modeled CSFDs that would be expected for surfaces with different ages, modeled CSFDs are made by combining an expected proportionality of craters of different sizes (a so-called "production function") with an estimate of past crater production rates (a so-called "chronology function"). Production and chronology functions are calibrated for the Moon, and are extended to other celestial bodies, including Mars (Ivanov, 2001).

We synthesized crater size-frequency distribution samples for our coupled delta-cratering model via Monte Carlo simulation, following the approach of Michael et al. (2016). We selected the Hartmann and Neukum (2001) Mars chronology function and Ivanov (2001) Mars production function for simulation. Monte Carlo simulations begin during the era of vigorous hydrological activity on ancient Mars at 3.5 Ga (Fassett & Head, 2008; Hoke & Hynek, 2009; Mangold et al., 2012), and include craters in the diameter range 10–300 m. Notably, the lower bound of our crater size range of interest extends beyond the size range of our chosen production function (Figure 2b; Ivanov,

2001); over this extrapolated diameter range, the slope of the production function is consistent with diameters within the function valid range (Figure 2b).

Monte Carlo simulation proceeds by choosing a crater size from a uniform probability distribution over the size range of interest, and determining the instantaneous cratering rate for that crater size from the chronology and production functions. The time to the next cratering event depends on the selected crater size, such that over many crater iterations, the synthesized crater size-frequency distribution conforms with the production function, and the distribution is consistent with a specified amount of elapsed time (Figure 2c). We specify CSFDs that represent elapsed time of 1, 10, and 100 Myr for simulations (Figure 2c).

We limited crater production to diameters less than 300 m because larger features can generate morphodynamic instability in the numerical delta model. We expect that this is a reasonable upper bound for craters that may be partially reworked by fluvial activity, but are unlikely to be completely eliminated from the stratigraphic record; this assumption will be tested with simulations.

2.2 Delta model

Coeval delta and crater production was simulated with the *pyDeltaRCM* numerical model (Moodie et al., 2021), which is a flexible implementation of the widely used DeltaRCM delta model (Liang et al., 2015a). DeltaRCM model design has been robustly validated (Liang et al., 2015a, 2015b, 2016) and used to examine delta morphology and evolution under various external forcings and processes (Lauzon & Murray, 2018; Lauzon et al., 2019; Piliouras et al., 2021; Moodie & Passalacqua, 2021; Hariharan et al., 2021, 2022, 2023). In this article, we do not describe the complete model implementation, and instead provide a high-level overview that highlights model components relevant to our study design and interpretations; a full model description is given in Liang et al. (2015a).

In DeltaRCM, a deltaic landform emerges from rules that iteratively route water and sediment via weighted random walk, from a fixed inlet location and into an initially empty receiving basin (Figure 3a; Liang et al., 2015a). Water is steered primarily by topographic gradients, moving down-gradient, and sediment is routed according to topographic and hydrodynamic gradients, with weighting that varies between the two for different sediments (Liang et al., 2015a; Wright et al., 2022). In this way, the routing rules were developed with "just enough" complexity to yield realistic fluvial-deltaic channel dynamics, so that the model maintains simplicity and computational efficiency (Liang et al., 2015a). Importantly, the dependence of water and sediment routing on topography is the fundamental connection between crater formation and delta evolution, and ultimately crater preservation or removal. DeltaRCM creates both fluvial and deltaic deposits simultaneously across the model domain (Hariharan et al., 2021); we do not differentiate between these depositional styles in assessing reworking bias, and discuss some potential implications of deltaic versus fluvial processes on our results in Section 4.3). We did not modify any model routing rules for this study, including adjustments to the effect of gravity on sediment suspension and transport (Supplementary Materials; e.g., Braat et al., 2023). Because the DeltaRCM model is governed by feedbacks between flow and topography, it can be applied to study crater preservation on Mars; other science applications of the model on Mars may require a careful sensitivity and parameter analysis.

DeltaRCM is known to be underestimate non-local and backwater hydrodynamic effects that develop upstream of channel bifurcations and obstructions (Liang et al., 2015b). As a result, water and sediment are erroneously transported up-slope in some uncommon circumstances where flow energy is especially high; in that case, high topography outside of channels may be unrealistically

lowered. This model idiosyncrasy leads to craters erroneously classified as having been partially reworked, but is a relatively rare occurrence, so we do not expect a significant impact on our results.

The mixture of sediment grain sizes input to a river delta is known to impact delta morphology and dynamics (Edmonds & Slingerland, 2010), and this dependence is borne out in DeltaRCM as well (Liang et al., 2015a, 2016; Hariharan et al., 2021; Moodie & Passalacqua, 2021). In DeltaRCM, the sediment mixture is controlled by a "sand fraction" parameter that shifts the mixture from muddy to sandy, and therefore transitions the delta between two modes of channel mobility. Channels in muddy simulations are generally stable, exhibiting a single active channel with moderate local lateral migration of channel bends, that is punctuated by large delta-scale lobe-switching avulsions that swiftly relocate the channel across the delta. In contrast, sandy simulations maintain multiple simultaneously-active channels that extensively migrate and frequently avulse across the landscape at multiple spatial scales (Liang et al., 2015a). Additionally, muddy simulations exhibit higher surface roughness, that is, higher average elevation variation across the landscape (Liang et al., 2016), which means that avulsions in muddy simulations develop new channels unevenly and in deep topographic lows, whereas avulsions in sandy simulations distribute sediment more evenly across the landscape. Importantly, this change in surface channel mobility translates to increased reworking of sedimentary deposits and stratigraphy for sandy simulations, relative to muddy simulations (Hariharan et al., 2021).

pyDeltaRCM uses a flow intermittency assumption to represent only morphodynamically active time, and therefore decrease model computation time. This common modeling assumption (e.g., Parker, 2004) is based on the nonlinear relationship between water and sediment discharge, and the increasing rarity of flows of increasing magnitude (Wolman & Miller, 1960). In essence, there is a river discharge that moves significant sediment volumes and occurs frequently, such that this discharge is treated as the meaningful control on the long-term evolution of the landform; only this discharge is modeled and is scaled to represent elapsed total time. Flow intermittency on Mars is poorly constrained (Stucky de Quay et al., 2021; Buhler et al., 2014), so model design simply assumes that significant flow intervals are evenly distributed over the duration of the simulation (e.g., not randomly distributed, but divided evenly over 100 Myr of elapsed total time).

In our simulations, water and sediment debouch into the 6 m deep receiving basin from a 6 m deep and 150 m wide channel at 1,350 m^3/s and 1.35 m^3/s discharge, respectively. The model uses a grid spacing of 20 m, over a 6×12 km domain. Simulations use a moderate sediment composition value, with equal parts sand and mud (i.e., sand fraction value is 0.5), which is within the broad range of grain size mixtures observed on Earth and Mars (J. P. Grotzinger et al., 2015; Stack-Morgan et al., 2023). These simulation parameters lead to development of channels 118 ± 68 m wide and 7 ± 3 m deep (mean $\pm$ standard deviation) that exhibit dynamics consistent with real-world terrestrial systems (Liang et al., 2015a, 2016). We ran simulations for 10,000 timesteps, which amounts to 107×10^6 seconds of intermittent bankfull river flow. Parameters and domain scaling were selected based on prior experience with numerical stability in the model, and minimal deviation from a set of parameters commonly used with DeltaRCM (e.g., Liang et al., 2015a; Lauzon & Murray, 2018; Lauzon et al., 2019; Piliouras et al., 2021; Moodie & Passalacqua, 2021; Hariharan et al., 2021, 2022, 2023). At the end of the simulation, deposits extend 4–5 km into the basin and span 8–10 km perpendicular to the inlet channel (Figure 3e), therefore maintaining an approximately axisymmetric planform over many cycles of channel movement (Parker et al., 1998; Reitz & Jerolmack, 2012; Moodie et al., 2019).

The model domain size and initial configuration, with a flat basin and single narrow inlet (Figure 3a) is conceptually consistent with a delta forming on the floor of a large crater (>30 km

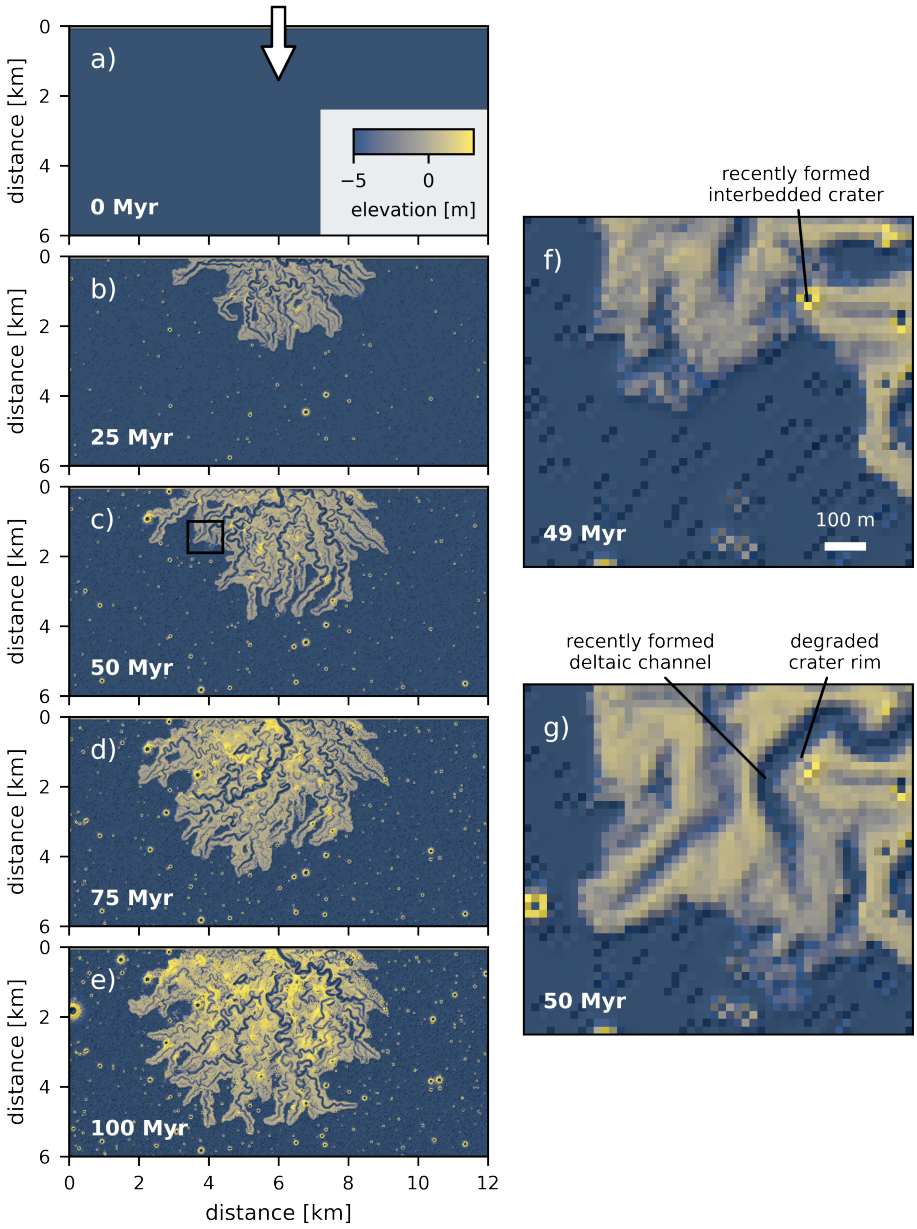

Figure 3. a–e) Timeseries of coeval river-delta and crater production for one 100 Myr simulation; color from blue to yellow highlights delta elevation. f–g) Highlight from timeseries at 49 to 50 Myr, showing a fluvial channel formed via avulsion and the associated partial degradation of an older crater ∼20 m in diameter; location of highlighted area is shown by black square in panel c.

diameter) from an inlet valley cutting across the crater rim. Notably, delta deposits at the end of simulation (Figure 3e) scale similarly to the Jezero Crater western delta deposits (e.g., Fassett & Head III, 2005; Goudge et al., 2018), though we did not explicitly attempt to model these deposits.

2.3 Coupling cratering and the delta model

Before beginning a simulation, we generate a crater-size distribution commensurate to the timescale of interest (e.g., 100 Myr) and determine independent crater formation times (i.e., cratering is a random Poisson process Herkenhoff & Plaut, 2000; Michael et al., 2016). Craters are placed between delta-model timesteps (Figure 3a–e), and are located randomly within the model domain but rectified to the model grid. Fresh crater geometry is generated according to (A. D. Howard, 2007), with the modification that ejecta deposits are not modeled beyond $6\times$ the crater radius. Crater formation is instantaneous, and has no effect on sediment erodibility in the delta model. Craters $\lesssim$40 m (i.e., $\lesssim 2\times$ the grid spacing; Shannon, 1949) have shorter rim heights in our model than dictated by A. D. Howard (2007), due to grid discretization effects (Supplementary Materials). This discretization effect could artificially increase the ability of smaller modeled craters ($\lesssim$ 30 m) to be removed, versus larger craters. However, because channel depths overwhelm crater rim heights in this size range, we do not expect discretization effects to affect our conclusions (Supplementary Material).

Each crater rim and ejecta deposit is tagged with a unique identifier, so that these materials are identifiable in the final modeled stratigraphy (Figure 4b). Rim material is labeled from $0.9r \leq x < 1.41r$, where r the crater radius and x is distance from the crater center, and crater ejecta is labeled from from $1.41r \leq x \leq 6r$. A single exception is that a minimum one-cell-wide annulus is created around a minimum one-cell central crater-floor cell; i.e., for the smallest craters, there is a single crater-floor cell with the eight surrounding neighbor cells marked as crater rim deposits. Rim and ejecta locations are tagged when craters are formed, and recorded to the model output intermittently. We use *DeltaMetrics* to convert timeseries model outputs to a gridded stratigraphic volume with 10 cm vertical resolution. *DeltaMetrics* determines the time when a given grid elevation was last occupied by the sediment surface at that location (Schumer et al., 2011), and assigns each voxel within the stratigraphic volume to reflect the appropriate simulation conditions. This approach creates a temporal discretization bias, that is minimized by saving model states at a high temporal resolution with respect to landscape evolution (e.g., Moodie et al., 2021; Moodie & Passalacqua, 2021; Hariharan et al., 2023).

Simulations do not include any additional surface processes that would eliminate crater deposits or obfuscate crater rims and reduce mappability, including for example, diffusive rim degradation by wind, water, or subsequent impactors (Öpik, 1966; Hartmann, 1966; Ross, 1968; Soderblom, 1970; Hartmann, 1971; Schultz & Gault, 1975; Hartmann & Neukum, 2001; A. Howard, 2004; Richardson et al., 2004, 2005; M. R. Smith et al., 2008; Richardson, 2009; Minton et al., 2015). However, our model implicitly includes crater obliteration by direct overprinting from subsequent craters (Woronow, 1977, 1978; Minton et al., 2015); we determined there to be little effect on our results from crater obliteration (Supplementary Material). Moreover, our modeling represents a net-depositional environment, and so assessment of crater removal in this study is not applicable to net-erosional valley networks on Mars, or locations without any evidence for fluvial and deltaic sedimentation.

We ran nine replicate simulations for each of 1 Myr, 10 Myr, and 100 Myr (27 simulations total) to assess uncertainty and develop a large number of craters for analyses (180,844 craters).

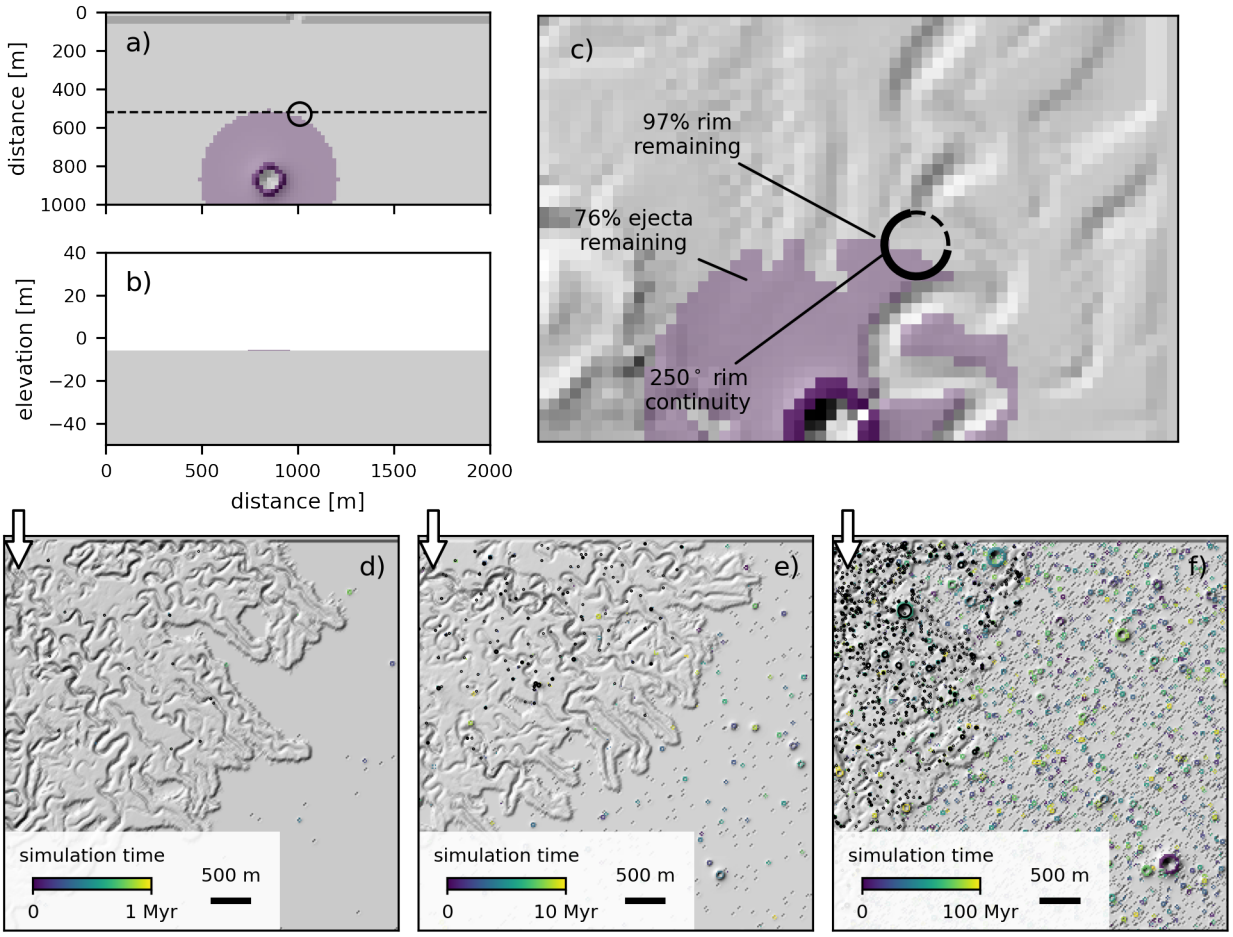

Figure 4. Example of a single pristine crater in a) mapview and b) cross-section, showing the extent of deposits tagged as crater rim (dark purple) and crater ejecta (light purple). c) Example of crater rim and ejecta degraded by fluvial reworking, and study metrics evaluated for this degraded crater. Topographic hillshade of a d) 1 Ma, e) 10 Ma, and f) 100 Ma simulation. Crater rim material *at the deposit surface* is colored by crater formation time, with black circles highlighting interbedded crater rims. The area of each panel is ~27 km^2 (approximately half of the model domain, with white arrows indicating the channel inlet location.

Model replicates for a given delta formation timescale (e.g., all 100 Myr replicates) used different crater-size distributions synthesized by Monte Carlo simulation.

3 Results

3.1 Crater rims and ejecta preserved in stratigraphy

Landscape development over time (Figure 3) generates stratigraphy that includes fluvial deposits and crater rim and ejecta material (Figure 4). From 180,844 craters across all formation duration and replicate simulations, we identified 26,709 interbedded craters. Iterating over each crater, we identified the initial crater deposit annulus area (i.e., excluding the crater floor), separated the rim and ejecta material, and calculated 1) the remaining fraction of rim annulus area, 2) the remaining fraction of ejecta annulus area, and 3) the angle subtended by the largest contiguous segment

of the rim annulus remaining (e.g., Figure 4c). For calculation of the remaining rim fraction for a single crater, for example, we divide the number of model grid cells that include rim material from that crater at any height in the stratigraphic column, by the number of grid cells that were initially marked as containing crater rim material for that crater; the remaining ejecta fraction is calculated in the same manner. Calculation of the preserved rim continuity similarly identifies grid cells with stratigraphic columns including rim material of that crater, and bins these cells into azimuthal ranges with respect to the crater center, and determines the arc length of the largest sector of consecutive bins. Identifying crater rim and ejecta material anywhere in the stratigraphic volume, rather than only exposed at the surface, isolates metrics from the effects of exhumational bias (Warren et al., 2019).

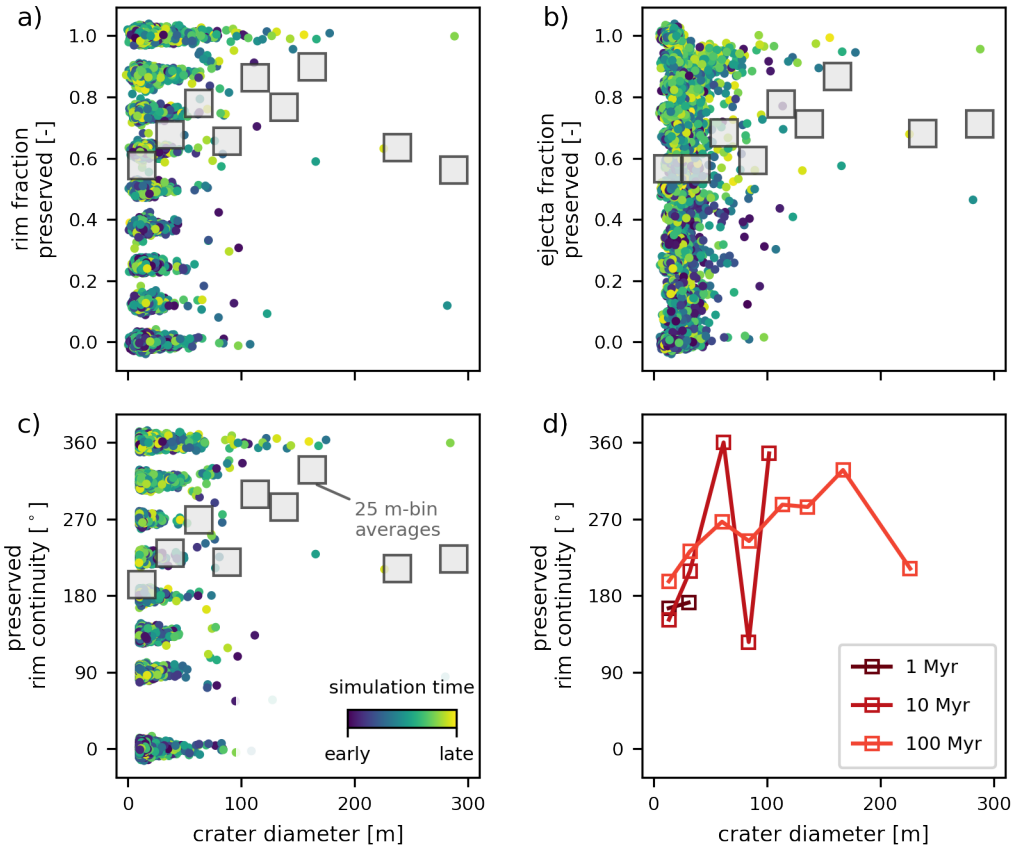

Figure 5. Interbedded crater a) rim fraction preserved, b) ejecta fraction preserved, and c) preserved rim continuity as a function of crater diameter, and colored by crater formation time within a simulation. Data are aggregated across all simulation timescales and replicates, and have normally-distributed noise added to both axes for visualization (mean of 0, and standard deviation of ± 0.01 or $\pm 1.5°$, and ± 1.5 m). Gray boxes mark non-overlapping 25 m-bin averages. d) 25 m-bin averages of preserved rim continuity separated by simulation duration. Total number of craters accumulated (i.e., simulation duration) does not impact the fluvial reworking bias.

All metrics are impacted by model grid discretization effects, but these effects are most apparent for smaller craters, and for the rim fraction and rim continuity metrics. This sensitivity arises because smaller crater rims occupy only eight grid cells immediately surrounding a single crater-floor grid cell, which creates, for example, just nine possible quanta for the preserved rim fraction

$(0, 0.125, \ldots, 0.875, 1.0$; Figure 5a); in some rare circumstances, time discretization effects introduce additional possible quanta (Supplementary Material).

For crater diameters from 10 to $\sim$50 m, the fraction of crater rim and ejecta area preserved varies between 0.0 and 1.0 (i.e., fully eroded to fully preserved), and this variability decreases as crater diameter increases, generally converging towards full preservation (Figure 5a,b). Preserved rim continuity is similarly variable for smaller crater diameters ($\lesssim$50 m), and converges towards 360° continuity with increasing crater diameter (Figure 5c). Importantly, robust trends in preservation for larger diameter craters in the size range of interest (150–300 m) are obscured by the fact that simulations included only seven craters larger than 150 m, due to the nature of crater production functions (e.g., Figure 2; Ivanov, 2001).

Non-overlapping 25 m crater diameter bin averages (gray boxes, Figure 5a–c) show a broad increase in preservation with increasing crater diameter. Approximately 67% of smaller interbedded-crater rims ($\lesssim$50 m) have been at least partially eroded (measured as rim continuity $<360°$), with 38% having less than half of the rim area remaining, and 44% having less than 180° of preserved rim continuity. Interestingly, about 53% of larger interbedded-crater rims (crater diameter $>$50 m) were also partially eroded (measured as rim continuity $<360°$), with 19% and 24% having less than half rim fraction preserved and less than 180° preserved rim continuity, respectively. Overall, simulations indicate that fluvial reworking can erode a substantial fraction of interbedded crater rims, especially affecting smaller crater rim deposits.

Preservation does not depend on the crater accumulation time duration (Figure 5d), or on crater formation time (Figure 5a–c). When preserved rim continuity data are separated into simulations representing 1, 10, and 100 Ma and summarized as 25 m-bin averages (Figure 5d), the trend of each simulation duration set is not distinguishable from the others. Most importantly, for smaller diameter craters ($\lesssim$50 m) where data density sufficiently characterizes fluvial reworking bias, there is little difference in rim continuity for different simulation durations (Figure 5d).

3.2 Biased crater size-frequency cumulative distributions

We made synthetic fluvial reworking-biased crater diameter distributions by Monte Carlo sampling from the simulated crater record, and compare biased distributions to the full interbedded crater distribution, and to the observed Mars interbedded crater distribution (e.g. Kite et al., 2014). To generate a CSFD biased by fluvial reworking, we randomly selected 56 craters from the simulated interbedded crater record (56 is the number of craters observed in the Kite et al. (2014) dataset), and excluded those craters with $<180°$ rim continuity. We repeated this process 100 times to assess distribution variability, and show the median distribution, and 16^{th} to 84^{th} percentile distributions in cumulative probability space, as a solid line and shaded envelope, respectively (Figure 6). Cumulative distributions are useful to visually highlight (dis)similarity of two distributions as (non)overlapping lines when plotted (Figure 6); differences in either distribution support (left-to-right shifts) or density (curve and slope change) create perceptual dissimilarity. Synthetic distributions reflect a set of "mappable" craters, which are those with rim preservation above a threshold value and anywhere in the simulated stratigraphic volume; we include craters embedded within the stratigraphy to isolate the fluvial reworking effect on crater distributions. We note that a $<180°$ rim continuity threshold was also used by Kite et al. (2014) to map craters on Mars, but Warren et al. (2019) excluded craters with $<150°$ of topographically elevated rim (including discontinuous sections); we thresholded based on continuous rim arc length because it is considerably simpler to implement for automatic calculation than other crater metrics. Sensitivity testing revealed that differences in the threshold (120°–240°) and the number of craters (40–72) do not impact results.

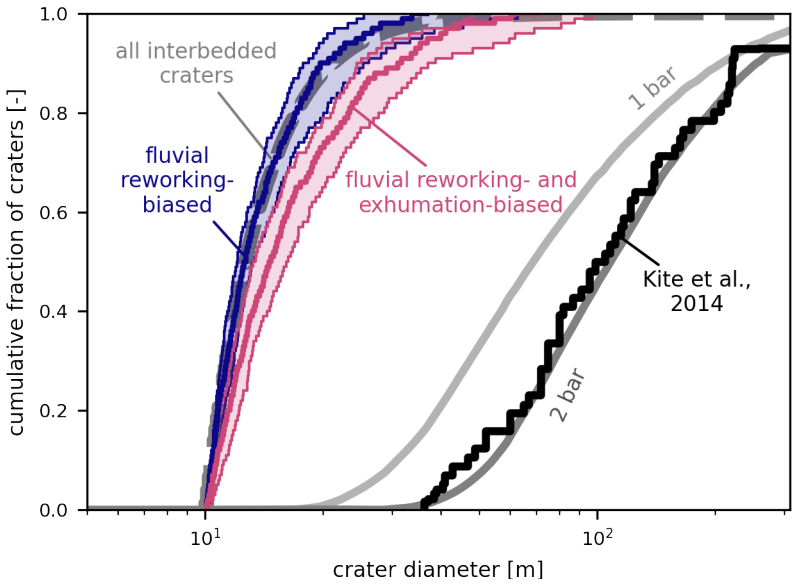

Figure 6. Empirical crater size distributions of all modeled interbedded craters (dashed gray line), preserved and mappable craters after applying fluvial reworking bias (blue) and fluvial plus exhumation biases (pink), and interbedded craters mapped by Kite et al. (2014) (solid black line); results are compared to crater size distributions predicted for paleo-atmospheric pressures (solid gray lines) from (Kite et al., 2014). For preserved and mappable crater size distributions, the biases applied are fluvial reworking (blue), and fluvial plus exhumational bias (pink). Calculated distributions are shown by the median (solid line), and envelope from the 16th to 84th percentile distributions (shaded area).

The cumulative distributions biased by fluvial reworking are similar to the cumulative distribution of all interbedded craters (Figure 6). Additionally, there is little variability among the sampled fluvial reworking-biased distributions (i.e., between the 16th and 84th percentile distributions; Figure 6). The sampled fluvial reworking-biased distributions have a distinct range and density from the Kite et al. (2014) observed crater diameter distribution (Figure 6). For example, the fluvial reworking-biased distributions are dominated by crater diameters 10–20 m approximately following an exponential distribution, whereas the observed data approximately follows a one-sided truncated normal distribution with the smallest observed diameter ∼35 m (Figure 6).

In addition to fluvial reworking, measured interbedded crater-size distributions are biased by exhumational processes that preferentially expose larger craters buried within stratigraphy (Kite et al., 2013). Preferential exhumation is due to geometric constraint that a quasi-horizontal plane cutting through a rock volume will sample features from the volume proportional to the features' length scale along the axis normal to the quasi-horizontal plane (Russ, 1986; Yielding et al., 1996). Assuming semi-hemispherical craters with a fixed ratio between crater diameter and depth (e.g., Melosh, 1989), the proportion of craters sampled on a quasi-horizontal plane is therefore dependent on crater depth (i.e., the vertical crater length; Lewis & Aharonson, 2014), or following the fixed depth-diameter ratio, crater exhumation bias is proportional to crater diameter (Kite et al., 2014). Our study examines crater rim and ejecta deposits, and we similarly assume a fixed ratio between crater depth and rim height, such that exhumation bias is linearly proportional to crater diameter. Note, the crater depth/height-to-diameter ratio is not explicitly included in the proportionality, so the relevant assumption is just that this ratio is fixed over the size range of interest.

We model exhumation bias by applying an increased weighting to larger craters in Monte Carlo sampling to generate synthetic crater diameter distributions from simulations. Probability for a crater with diameter d to be included in the synthetic distribution goes as $p(d) \propto d/d_{min}$, where $d_{min} \approx$10 m is the smallest crater diameter in the simulations. We empirically tested whether exhumational bias follows this proportionality, and determined that it is a reasonable first-order approximation of the bias imparted by exhumation, but that bias depends on the relative rate of deposit accumulation and crater production, and assumptions of crater geometry (Section 4.4.3; Supplementary Materials).

Cumulative distributions biased by fluvial reworking and exhumation have a marked increase in larger craters, with respect to the distribution of all interbedded craters (Figure 6). Still, the distributions are dominated by 10–30 m diameter craters, and remain substantially different in shape and scale from the observed crater-size distribution (Figure 6).

4 Discussion

4.1 Fluvial reworking bias does not explain observed crater populations

Despite nearly half of smaller craters ($\lesssim$50 m) having $<180^\circ$ remaining rim continuity and potentially not being mappable, the shift in the cumulative CSFD due to fluvial reworking is very small (Figure 6). This small shift arises because the CSFD is dominated by smaller craters: there are $\sim$340 times more interbedded and mappable ($>180^\circ$ rim continuity) craters sized 5–15 m than sized 55–65 m (18,743 and 55 craters, respectively). The relative abundance of smaller craters is a factor of the crater production function, and although the true crater production function is unknown, the approximately exponential form of the function is not disputed (Fassett, 2016). So, although fluvial reworking can remove many smaller craters, the dominance of smaller craters in the CSFD is inescapable, and fluvial reworking cannot bias the crater record to the extent needed to explain observed distributions. Notably, even in the extreme case of a delta formed over 1 Myr, which leads to the smallest number of accumulated craters (Figure 2), fluvial reworking does not modify the CSFD enough to match observations on Mars (Figure 5d; Supplementary Material).

Our findings are consistent with previous studies that hypothesize fluvial reworking is not a primary control on observable crater size-frequency distributions of ancient interbedded craters on Mars (Kite et al., 2014; Warren et al., 2019). Our results indicate that fluvial reworking is a subordinate control because of the overwhelming number of smaller craters generated, rather than the notion that crater deposits are not eliminated from the stratigraphic record (indeed, many crater deposits are eliminated by fluvial reworking; e.g., Figures 3 and 5). Though lateral migration and avulsion place channels across the entire delta over time, channels occupy only a small fraction of the delta surface at any moment in time (Reitz & Jerolmack, 2012), such that the majority of new interbedded craters are formed away from active channels. Interestingly, a crater must be at least partially buried by fluvial sediments to be considered an interbedded crater for this study, so it appears that craters formed away from active channels receive distally deposited fine sediment, but that many crater locations must not be revisited by a channel during the simulation. In summary, our simulations show that fluvial reworking, by way of lateral migration and avulsion, is not able to remove smaller craters at the pace they are created.

Our conclusions bolster studies that use the lack of smaller interbedded craters as evidence for a higher pressure ancient atmosphere. In contrast to migrating rivers that intermittently visit locations on the landscape, a planetary atmosphere exists everywhere above the landscape and is in place to brake and ablate all incoming impactors. For example, in the case of an atmosphere with

stable pressure, there is a lower limit to the diameter of impactors that survive atmospheric ablation, translating to a lower limit on crater diameters formed (Kite et al., 2014). Though paleo-pressure may have fluctuated in the past (Warren et al., 2019), we see very little possibility for atmospheric pressure to have remained low enough for long enough that a substantial number of smaller craters would have formed *and* subsequently be eliminated by fluvial reworking. Instead, a more likely scenario is that the smaller craters never formed, due to higher atmospheric pressure. Moreover, the sustained and intense fluvial activity that would be needed to rework enough smaller craters to reproduce observed distributions would be highly unlikely without at least some atmosphere (e.g., Kite, 2019; Kite et al., 2022), which would therefore inhibit formation of smaller craters in the first place. In summary, simulation results indicate that although rivers are sometimes in the right place to remove smaller craters, an atmosphere is always in place to remove small impactors and prevent formation of smaller craters altogether.

4.2 The functional form of the fluvial reworking filter

Although fluvial reworking cannot account for the lack of smaller interbedded craters observed on Mars, our modeling results indicate that fluvial erosion can remove a significant proportion of these craters from the stratigraphic record. Creating a well-calibrated crater removal function could bolster atmospheric paleo-pressure interpretations. Moreover, a set of calibrated crater removal functions could be used to infer characteristics of ancient river migration and avulsion, for example, from divergences between observed CSFDs and those predicted for atmospheric filtering from an independently constrained paleo-pressure. It would be problematic to calibrate a crater removal function from our simulation results heretofore, because simulations include a limited number of larger interbedded crater observations (only seven craters $\gtrsim$150–300 m; Figure 5). The limited number of larger craters is a realistic constraint, imposed by the nature of crater production in the solar system (e.g., Figure 2b,c; Ivanov, 2001), but relaxing this constraint could refine our view of crater reworking over the complete range of crater sizes of interest (10–300 m).

4.2.1 Uniform crater size-frequency distribution simulations

To increase observations of interbedded craters $\gtrsim$150 m in diameter, We ran additional simulations with a uniform crater size-frequency distribution (i.e., craters of all diameters 10–300 m are equally likely). Simulation parameters otherwise remained the same as previous simulations, except for two modifications. First, we limited the number of craters per simulation to 250 and increased the number of replicate simulations, because too many larger craters in a single simulation introduced numerical instability to the delta model. Second, we varied sediment composition input to the delta (Liang et al., 2016; Moodie & Passalacqua, 2021), to assess how channel mobility modulates the fluvial reworking filter. We varied the input sediment mixture from a muddy to sandy composition (sand fraction 0.2, 0.5, and 0.8) across 36 runs (12 replicates for each sand fraction), yielding 9000 craters and 1180 interbedded craters to examine preservation metrics (Figure 7). Sediment composition is known to influence channel dynamics and the resultant bias in stratigraphic preservation (e.g., Straub et al., 2015), so this parameter is highly relevant to our study and will set first-order bounds on plausible interbedded crater reworking.

We computed the rim fraction preserved, ejecta fraction preserved, and rim continuity in the same manner as previous simulations (Figure 7a–c). Similar to size-frequency distribution simulations, uniform size distribution simulations indicate varied preservation, ranging from undegraded craters to complete removal. 25 m-bin averages indicate that preservation generally increases with crater size (Figure 7a–c). Notably, uniform size distribution simulations characterize average fluvial

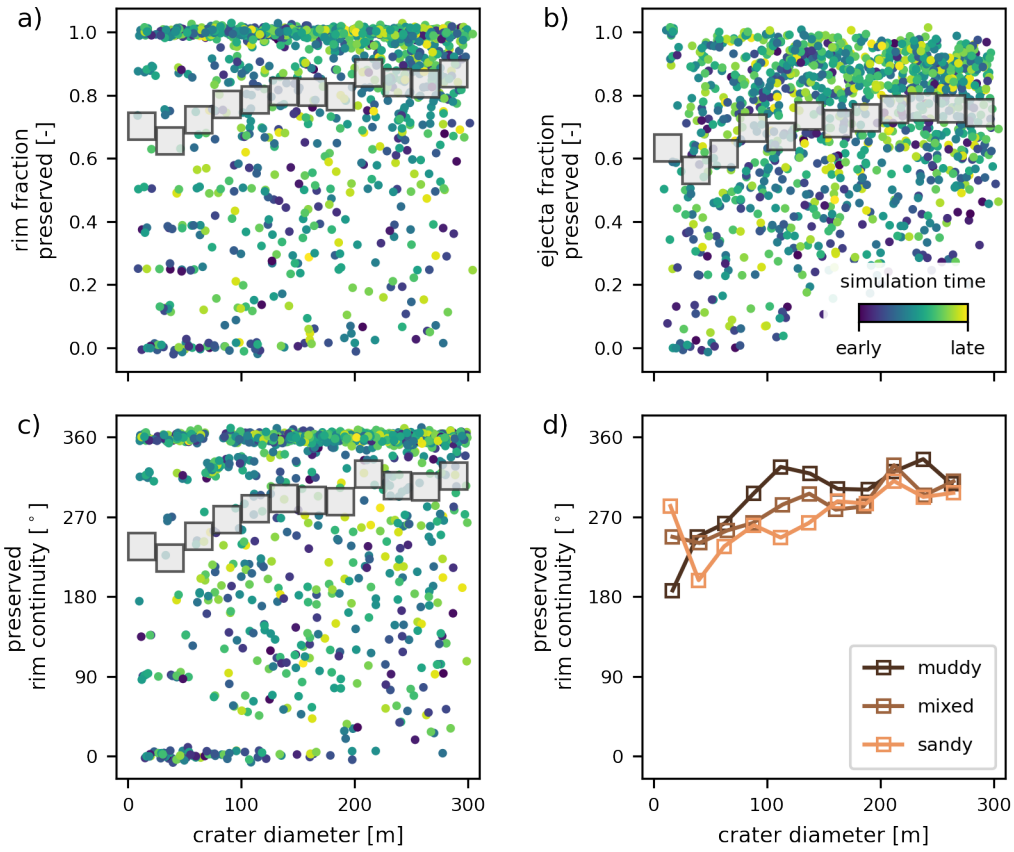

Figure 7. Interbedded crater a) rim fraction preserved, b) ejecta fraction preserved, and c) preserved rim continuity as a function of crater diameter for uniform crater size-frequency distribution. Data are aggregated across all input sediment compositions and replicates, and up to ± 0.1 or $\pm 1.5^{\circ}$ and ± 1.5 m point jitter is added for visualization. Gray boxes mark mutually exclusive 25 m-bin averages. Calculated metrics show that preservation is varied, but on average increases with increasing crater diameter. d) 25 m-bin averages of preserved rim continuity separated by sediment composition input to the delta. Increasing input sandiness led to a decrease in preserved rim continuity, i.e., an increase in fluvial reworking bias.

reworking bias more smoothly and over a more complete crater diameter range than size-frequency distribution simulations (Figures 5 and 7).

Splitting simulations by input sediment composition reveals differences in average preservation of smaller crater deposits (Figure 7d). Muddy simulations resulted in higher preservation than sandy simulations on average (Figure 7d). Average preservation in muddy simulations shows a nonlinear dependence on crater diameter (with preservation dropping steeply below $\lesssim$100 m), whereas sandy simulations have an approximately linear dependence on crater size (Figure 7d). As described in Section 2.2, DeltaRCM simulations of sandy deltas have higher rates of channel mobility and therefore increased sediment reworking relative to muddy deltas (Liang et al., 2015a; Hariharan et al., 2021). Differences in fluvial reworking for different sediment compositions are second order to the size-dependent trend, and are consistent with a process-based understanding of channel dynamics and stratigraphic preservation (Hajek & Straub, 2017; Hariharan et al., 2021).

4.2.2 Calibrating a function for crater removal by fluvial reworking

We define a filtering function, representing the average bias applied to the interbedded crater record by fluvial reworking:

$$c = (1 - c_0)\left[1 - \exp\left(\frac{(d_0 - d)}{n}\right)\right] + c_0, \quad (1)$$

where c is the fraction of craters of diameter d remaining, c_0 is a reference crater fraction remaining when $d \to 0$, d_0 is a reference crater diameter, n is an "e-folding" crater diameter. The functional form of the filter is after the Warren et al. (2019) crater removal factor, and is augmented with a reference term c_0 to represent the fraction of craters preserved as $d \to 0$. Values of c_0 are bounded in $[0,1]$, values of d_0 are bounded in $[0,\text{inf})$ (Warren et al., 2019), and Equation 1 is only valid for $d > 0$, such that values of c are always in $[0,1]$. Note that when $c_0 = 0$, the original filter function of Warren et al. (2019) is recovered.

The constraint that d_0 characterize a reference crater diameter ≥ 0 forces the average remaining crater fraction c to be zero for $d \geq 0$ (i.e., full reworking reached at some crater diameter greater than or equal to zero, Figure 8). However, there is no empirical evidence or theory that indicates full reworking should be a requirement of the fluvial filter. Indeed, our empirical simulations show only partial reworking for the smallest crater diameters (e.g., $c > 0$ as $d \to 0$; Figure 7), and therefore do not support the constraint imposed by the d_0 reference diameter. One option would be to allow d_0 to take a negative value, but the physical meaning of a negative reference diameter is not clear. Instead, we choose to augment the filter function with the c_0 term, to ensure $d_0 \geq 0$ and enable partial reworking as $d \to 0$.

Figure 8 shows Equation 1 determined with parameters from Warren et al. (2019) for Meridiani ($c_0 = 0$, $d_0 = 15.7$, $n = 23$), and for parameters determined from regression for our simulation results. For regression, we determine mappable fraction as the 25 m-bin averages of interbedded craters from the uniform crater size-frequency distribution simulations with rim continuity $\geq 180°$, and treating the muddy and sandy simulations separately (i.e., data are after Figure 7c). We used the uniform crater size-frequency distribution simulation results for regression because these results characterize average crater preservation across the crater size range of interest; only seven craters $\gtrsim$150–300 m were observed in the simulations using the Ivanov (2001) crater size-frequency distribution (Figure 5). Using different simulation results would yield different parameters for Equation 1, but we expect the model form would remain the same (e.g., compare figures 5 and 7). We defined the mappable crater fraction using the rim continuity data because this metric is commonly used as a threshold criteria in crater counting (Kite et al., 2014; Warren et al., 2019), and other metrics would be difficult to constrain outside of the model. Finally, we set $d_0 = 0$ and estimate c_0 and n only, because c is non-uniquely dependent on c_0 and d_0 (Equation 1). Model parameters determined for muddy simulations are $c_0 = 0.46 \pm 0.09$, $d_0 = 0$, and $n = 78 \pm 18$, and are $c_0 = 0.63 \pm 0.04$, $d_0 = 0$, and $n = 288 \pm 76$ for the sandy simulations; $\pm$ represent 1σ values.

The filter proposed by Warren et al. (2019) captures the nature of the relationship between fluvial reworking and average crater preservation, but their parameterization underestimates the range over which reworking occurs, and overestimates the degree to which reworking changes with crater diameter (Figure 8). Our calibrated models have a larger e-folding crater diameter (n), and because we set $d_0 = 0$ and determine c_0, our parameterizations maintain a proportion of potentially mappable craters (i.e., $c > 0$) at even the smallest crater diameters. Differences in crater preservation patterns between the muddy and sandy simulations lead to distinct estimated parameters for these sedimentological systems (Figure 8), though difference due to sediment input is small with respect

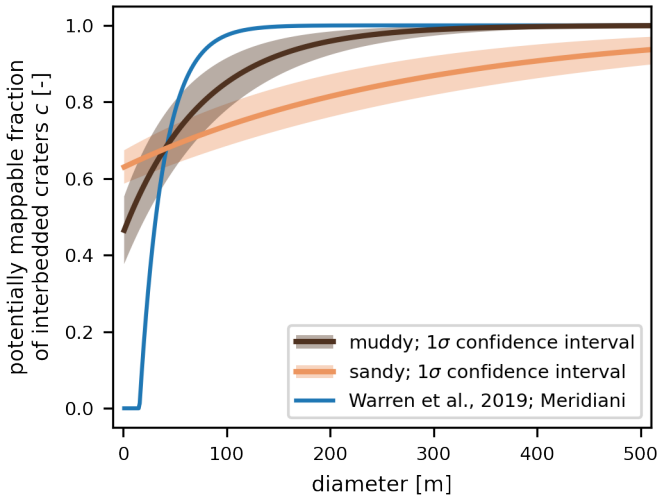

Figure 8. Potentially mappable fraction of interbedded craters as a function of crater diameter. The blue curve is Equation 1 with parameters from Warren et al. (2019) for Meridiani ($c_0 = 0$, $d_0 = 15.7$, $n = 23$). The brown and orange curves and shaded areas are Equation 1 evaluated with model parameters and 1σ confidence intervals for muddy and sandy simulations, respectively. Data used to determine parameters are 25 m binned averages fraction of craters preserved with $\geq 180^\circ$ rim continuity, and therefore includes buried craters (i.e., excludes exhumation bias).

to the difference from the Warren et al. (2019) parameterization. Estimated values of n characterize the sensitivity of reworking to change in crater diameter in Equation 1, with smaller values of n representing increased sensitivity in muddy simulations.

4.2.3 Implications and potential applications of the crater removal function

Fluvial reworking bias can be accounted for where a sufficient density of interbedded craters is present, and Equation 1 can therefore bolster atmospheric paleo-pressure interpretations. For example, Equation 1 can integrate into an inference framework that improves atmospheric paleo-pressure estimates, by considering the observed CSFD as it is found, after being biased by atmospheric filtering and fluvial reworking (in that order). This framework would shift interpreted paleo-pressure upper-bounds (e.g., Kite et al., 2014; Warren et al., 2019) to now-lower paleo-pressure estimates with meaningful uncertainty; for example, CSFDs modeled for different atmospheric pressures and fluvial reworking would steepen and rotate counter-clockwise, becoming increasingly convex-up at smaller diameters. We emphasize that our estimated fluvial reworking filter characterizes the fraction of craters preserved *on average* (with a measure of variability), and so any revised paleo-pressure interpretations using this filter should carry uncertainty due to variability (Figure 8). Additionally, our estimated fluvial reworking filter implicitly incorporates the effects of crater obliteration during formation of new craters, and so may slightly overestimate the effect of fluvial reworking bias alone (Supplementary Materials); we cannot separate crater obliteration from fluvial reworking in our simulations, as is the case in natural systems. To be complete, an inversion framework should incorporate additional crater-degrading surface processes and possible sources of bias (exhumation bias has already been incorporated in these frameworks; Kite et al., 2014); but importantly, we do

not expect these factors to significantly impact crater counts (Section 4.4). Finally, it is worth reiterating that our filtering model (Equation 1) is only applicable in net-depositional environments, and is not applicable in net-erosional valley networks on Mars, or locations without any evidence for fluvial and deltaic sedimentation.

Details of sediment composition and channel characteristics that prevailed on ancient Mars are not well constrained (J. P. Grotzinger et al., 2015; Stack-Morgan et al., 2023), so model-fit parameterizations should be interpreted as scenarios that estimate a plausible range of reworking bias. Interestingly, it may be possible to infer ancient channel dynamics from mapped CSFDs if atmospheric paleo-pressure is independently constrained. For example, the crater-diameter range over which the observed crater size-frequency distribution deviates from the known paleo-pressure expected distribution, could inform whether ancient channel dynamics were more similar to dynamics of channels in muddy or sandy simulations.

4.3 Crater removal determined by channel avulsion frequency and channel geometry

We interpret the difference in average preservation between muddy and sandy simulations to be due to varied channel mobility modes and varied channel geometry between the cases, which are well known to be modulated by the sand fraction input to DeltaRCM (Section 2.2; Liang et al., 2015a, 2016; Moodie & Passalacqua, 2021). To briefly summarize simulation differences, muddy simulations exhibit narrower and deeper channels that remain in place longer before delta-scale avulsions relocate channels, whereas sandy simulations maintain shallower and wider channels that frequently avulse at multiple scales. These model behaviors are consistent with a process-based understanding of controls on channel geometry (Dunne & Jerolmack, 2018; Dong et al., 2019; Dunne & Jerolmack, 2020) and avulsion (Mohrig et al., 2000; Slingerland & Smith, 2004; Straub et al., 2015).

We originally hypothesized that larger craters ($\sim$50–300 m diameter) have rims rising above the delta plain that would present a physical obstacle to flow, and therefore not be reworked and removed from the stratigraphic record. Our results repeatedly document a crater diameter-dependent bias (e.g., Figures 5 and 7), and here we interpret observed crater preservation patterns in the context of hypothesized topographic steering. It is important to emphasize that differences between muddy and sandy preservation are only apparent in *average* behavior (Figure 7d, Figure 8), and that both cases exhibit varied preservation ranging from craters that are fully eliminated to fully preserved.

Channel avulsions cause flow to spread across the delta landscape, generally following topographic gradients to a new outlet on the coast (Jerolmack & Paola, 2007; Reitz et al., 2010). In our simulations, flow during avulsion is steered by self-organized delta topography and by crater topography; an example of flow steered by self-organized topography during an avulsion is shown in Figure 3f–g. Infrequent avulsions in muddy simulations create significant self-organized topographic roughness (e.g., Liang et al., 2016), such that if flow encounters crater topography during an avulsion, it may be steered towards a nearby topographic low, wherein a new channel is formed (e.g., Figure 3f–g). Frequent avulsions in sandy simulations distribute sediment more evenly across the deltaic landscape, such that topographic lows are rapidly filled and topographic variability is relatively small (e.g., Liang et al., 2016). Therefore, when an avulsion occurs in sandy simulations, flow is not easily steered by crater topography towards a topographic low (i.e., because there are no significant topographic lows). The effect of these differences, on average, is that the overall crater removal fraction is higher in sandy simulations (Figure 8), and crater removal is less sensitive to crater size in sandy simulations (Figure 8). Said another way, the presence of topographic lows in

muddy simulations enhances the size-dependent bias that removes smaller craters from the crater record, but reduces reworking overall.

From a geometric perspective, fluvial reworking occurs where a channel cross-section intersects with deposited sediments, and so is limited to the landscape area visited by channels, and extends into the subsurface down to the channel depth. This perspective implies that more frequent avulsions would increase fluvial reworking, and also that deeper channels would increase fluvial reworking. Sandy simulations, which have shallower channels and more frequent avulsions than muddy simulations, exhibit higher average reworking. This indicates that crater deposit reworking is more sensitive to avulsion frequency than channel depth. We expect that processes influencing crater removal in uniform crater size-frequency distribution simulations also modulate reworking in our primary simulations with CSFDs synthesized from a production function. Reworking in primary simulations is likely transitional between reworking observed in end-member muddy and sandy simulations, because the input sand fraction value in these simulations is between the muddy and sandy sand fraction values.

There are some additional factors of the model design and simulation configurations that could affect reworking. Reworking could increase in a situation where a river or delta is confined by valley walls, because a higher proportion of the active fluvial area (i.e., floodplain) is occupied by channel area (Dong & Goudge, 2022). By similar logic, braided rivers that occupy a larger fractional area of the active fluvial area (Tejedor et al., 2022; Dong & Goudge, 2022) could show a higher proportion of crater reworking. Thus, we would expect the number of intersections between interbedded craters and channel cross sections to increase, thereby enhancing crater removal. Additionally, river bend migration in confined valleys can be dominated by down-valley bend translation that eliminates strata over the full valley width (Limaye & Lamb, 2013). However, it is not currently known whether Aeolis Dorsa, or other paleo-channel features were formed in confined valleys or on broad alluvial plains (Cardenas et al., 2017; Dong & Goudge, 2022).

4.4 Degradation, obliteration, exhumation, and image resolution as potential sources of bias

Crater degradation is the erosion of crater rims and infilling of crater floors by sedimentary processes, so that crater topographic expression is gradually diminished over time (Craddock et al., 1997; Forsberg-Taylor et al., 2004; M. P. Golombek et al., 2014). We did not include any crater degradation effects in our model, so a natural question is whether including these processes, in conjunction with fluvial reworking bias, could meaningfully impact the observable smaller crater record on Mars. In this section, we examine several processes and effects that alter crater topography on ancient and modern Mars. We comment on whether these processes could impact modeling results, and speculate on how sensitive counting of interbedded craters on Mars is to these processes.

4.4.1 Wind and aeolian erosion

M. P. Golombek et al. (2014) found that aeolian erosion degrades recently formed smaller crater rims on modern Mars at up to 1 m/Myr, but that this rate quickly declines to 0.1 m/Myr; longer-term rates are as low as 0.001 m/Myr (M. P. Golombek et al., 2006). Aeolian sedimentation rates during the period of fluvial activity of interest beginning 3.5 Ga are poorly constrained, but modern rates of erosion serve as a helpful proxy for the following thought experiment. For a crater rim height to diameter ratio of $\sim$0.04 (Pike, 1977; Melosh, 1989; Robbins & Hynek, 2012), we expect freshly formed crater rims $<$1 m high for craters smaller than 30 m. This rim height is

sufficiently small that wind-blown degradation rates up to 1 m/Myr could substantially weather craters before entering the stratigraphic record.

Our simulations spanned a range of plausible delta formation timescales 1, 10, and 100 My (Bhattacharya, 2005; Buhler et al., 2014; Irwin et al., 2015; Lapôtre & Ielpi, 2020). In the extreme case of a delta forming intermittently over 100 My and aeolian erosion occurring at similar rates to modern craters, a crater formed on the delta surface would be weathered for several million years before a channel returns to the area to potentially bury the crater deposit (Figure 3). In such a situation, it is possible that smallest-crater rims could be substantially degraded before being incorporated into the stratigraphic record, and therefore be unrecognizable as craters after exhumation. At more moderate timescales of delta formation and lower crater degradation rates, we do not anticipate that crater rims would be substantially degraded before potential incorporation into the stratigraphic record. Future modeling could consider how craters of varying degrees of degradation are incorporated into the stratigraphic record and later exhumed as landforms observable on the modern Mars surface (e.g., Cardenas et al., 2022). Importantly, even if wind degrades all or a significant fraction of craters below 30 m before burial, our conclusions would not change, because mappable cumulative crater-size distribution shape would likely still be dissimilar to Mars observations (e.g., Figure 6).

4.4.2 Crater obliteration

Obliteration of an existing crater rim or ejecta deposit by the formation of a new impact crater leads to a steady state crater size-frequency distribution, which deviates at smaller crater diameters from the distribution dictated by the crater production function (Woronow, 1977, 1978; M. R. Smith et al., 2008; Richardson, 2009; Minton et al., 2015). This crater obliteration processes is implicitly included in our simulations, though our simulations accumulate far fewer craters than needed to approach a steady state distribution. Nevertheless, we ran nine simulations without river-delta sediment input, and then generated craters according to 100 Myr of elapsed time beginning 3.5 Ga, and quantified preservation using the same routine as the main text. In these simulations, we find that smaller craters are preferentially rendered unmappable by obliteration (consistent with prior research), but that the magnitude of crater removal by obliteration is far less than fluvial reworking, and therefore does not affect our study interpretations. For example, crater obliteration removes $\sim$10% of crater rim area for craters $\lesssim$50 m, $\sim$10% of crater ejecta area for all crater sizes modeled, and similarly minimally impacts the preserved rim continuity. Importantly, these obliteration metrics represent upper bounds on crater obliteration bias, because craters remain at the modeled surface and there is no mechanism to incorporate crater material into stratigraphy and away from the surface new craters form on.

We do not expect that Mars interbedded crater records are significantly affected by crater obliteration during formation of new craters. Interbedded craters would have formed on active sedimentary surfaces that would not have persisted long enough for an equilibrium density of craters to form.

4.4.3 Exhumational bias of larger craters

Exhumational bias preferentially exposes larger craters, when a sedimentary volume with interbedded craters is eroded (Kite et al., 2013). To represent this process in our analysis, we relied on previous research that presents a geometry-based theory for how this bias impacts crater size-frequency distributions (Lewis & Aharonson, 2014). We attempted to empirically validate this theory in the course of our research, and found that the theory provides an acceptable first-order

approximation of the effect. Still, we determined that there is an opportunity for further research to improve our understanding of exhumational bias in crater records (Supplementary Material).

In any case, we do not expect that plausibly enhanced exhumational bias would impact our primary conclusion that fluvial reworking cannot reproduce observed Mars crater-size distributions. Our attempts to validate the exhumational bias theory indicate that the level of bias needed to remove enough smaller craters to explain the observed Mars crater record is not plausible. Importantly, an improved understanding of exhumational bias will be necessary to incorporate the fluvial reworking process into inference frameworks (e.g., Section 4.2.3).

4.4.4 Image and data resolution

Crater mappabilty is affected by horizontal and vertical image resolution, as well as image illumination angles (Williams et al., 2018). Craters smaller than $3\times$ data resolution (dx) are not reliably mapped (Richardson, 2009), which provides a reasonable estimate of the lower bound of potentially mappable craters in any dataset. Crater measurements generated by Kite et al. (2014) used HiRISE images (0.25–0.5 m/pixel) that yield gridded digital terrain models (DTMs) with approximately 2–3 m horizontal resolution, and vertical precision on the order of tens of centimeters (McEwen et al., 2007; Beyer et al., 2018). Freshly-formed crater rim heights are approximately 4% of the crater diameter (Robbins & Hynek, 2012), so craters $\geq$5 m would have rim heights $\geq$20 cm, and can be reasonably expected to be mappable in DTMs derived from HiRISE imagery. Therefore, we do not expect data resolution to impact mappable crater counts in previous Mars studies, but CSFDs generated without high-resolution images are unlikely to generate reliable paleo-atmospheric pressure estimates.

As mentioned previously, embedded craters that become exposed at the surface by exhumation could be degraded by aforementioned modern sedimentary processes (i.e., wind-blown erosion). Interestingly, these processes could render craters that are fully preserved in the fluvial reworking sense, to become unmappable at present day, due to post-exhumation erosion that lowers observable rim heights below image resolution thresholds. We cannot rule out that modern erosion of ancient interbedded craters affects mappable crater distributions on Mars (Williams et al., 2018), but also do not expect this effect to invalidate upper-bound paleo-pressure interpretations, because including potentially omitted smaller craters would lower upper-bound estimates.

5 Conclusions

In this study, we perform a quantitative evaluation of the potential for fluvial reworking of sedimentary deposits to impart a size-dependent bias on crater size-frequency distributions. Our modeling approach reveals that as many as 67% of smaller craters ($\lesssim$50 m diameter) are at least partially eroded, with 38–44% of smaller craters having less than half the initial deposit remaining, and that preservation of craters is highly variable. Notably, average crater preservation decreases with decreasing diameter, confirming the presence of a size-dependent fluvial reworking bias. However, the nature of crater size-frequency distributions (i.e., an approximately exponential increase in crater frequency with decreasing diameter) creates a condition where fluvial reworking cannot remove enough smaller craters to meaningfully bias interbedded crater records. That is to say, although fluvial reworking preferentially removes smaller crater deposits from the stratigraphic record, there are too many smaller craters produced for preserved crater size-frequency distributions to meaningfully change. This conclusion ultimately bolsters paleo-pressure studies that rely on these interbedded crater records. We developed a function that predicts the average fraction of craters removed by flu-

vial reworking, and determined parameters of the function for simulations exhibiting varied channel dynamics. Specifically, we observe that simulations with more sand input remove more crater rims overall, but with reduced size-dependent bias; we interpret these observations as being controlled by changes in avulsion frequency and topographic relief that depend on input sediment composition. Overall, our findings bolster studies that assert fluvial reworking is not a primary control on smaller interbedded crater counts on Mars.

Open Research Section

All data, custom model scripts, and analysis scripts used in this research are archived on the corresponding author's Github page at https://github.com/amoodie/paper_resources in a folder titled "Moodie_marscraterreworking". Upon acceptance of this article for publication, the authors will archive the aforementioned folder, along with complete copies of versioned models and bespoke software used in this research, in a Zenodo repository (doi 10.5281/zenodo.10050333).

Acknowledgments

The authors gratefully acknowledge David Mohrig for helpful conversations that guided this research. We are also grateful to two anonymous reviewers for their thoughtful comments and suggestions that greatly improved our manuscript. A.M. was supported by a Jackson School of Geosciences Postdoctoral Fellowship at the University of Texas at Austin.

References

Beyer, R. A., Alexandrov, O., & McMichael, S. (2018). The ames stereo pipeline: Nasa's open source software for deriving and processing terrain data. *Earth and Space Science*, *5*(9), 537–548. doi: 10.1029/2018EA000409

Bhattacharya, J. P. (2005). Dynamic river channels suggest a long-lived noachian crater lake on Mars. *Geophysical Research Letters*, *32*(10). Retrieved from `https://doi.org/10.1029/2005gl022747` doi: 10.1029/2005gl022747

Bishop, J. L., Fairén, A. G., Michalski, J. R., Gago-Duport, L., Baker, L. L., Velbel, M. A., ... Rampe, E. B. (2018, February). Surface clay formation during short-term warmer and wetter conditions on a largely cold ancient Mars. *Nature Astronomy*, *2*(3), 206–213. doi: 10.1038/s41550-017-0377-9

Braat, L., Brückner, M., Sefton-Nash, E., & Lamb, M. (2023, April). Gravity-driven differences in fluvial sediment transport fluxes on Mars and earth. *none*. doi: 10.31223/x5bq0r

Bridge, J. S., & Mackey, S. D. (1992). A theoretical study of fluvial sandstone body dimensions. In *The geological modelling of hydrocarbon reservoirs and outcrop analogues* (pp. 213–236). John Wiley & Sons, Ltd. doi: 10.1002/9781444303957.ch14

Buhler, P. B., Fassett, C. I., Head, J. W., & Lamb, M. P. (2014, October). Timescales of fluvial activity and intermittency in milna crater, Mars. *Icarus*, *241*, 130–147. doi: 10.1016/j.icarus.2014.06.028

Cabrol, N. A., Grin, E. A., Newsom, H. E., Landheim, R., & McKay, C. P. (1999). Hydrogeologic evolution of gale crater and its relevance to the exobiological exploration of Mars. *Icarus*, *139*(2), 235–245. doi: 10.1006/icar.1999.6099

Cardenas, B. T., & Lamb, M. P. (2022, October). Paleogeographic reconstructions of an ocean margin on Mars based on deltaic sedimentology at aeolis dorsa. *Journal of Geophysical Research: Planets*, *127*(10). doi: 10.1029/2022je007390

Cardenas, B. T., Lamb, M. P., & Grotzinger, J. P. (2022, October). Martian landscapes of fluvial

ridges carved from ancient sedimentary basin fill. *Nature Geoscience*, *15*(11), 871–877. doi: 10.1038/s41561-022-01058-2

Cardenas, B. T., Mohrig, D., & Goudge, T. A. (2017, 09). Fluvial stratigraphy of valley fills at Aeolis Dorsa, Mars: Evidence for base-level fluctuations controlled by a downstream water body. *GSA Bulletin*, *130*(3-4), 484–498. doi: 10.1130/B31567.1

Craddock, R. A., Maxwell, T. A., & Howard, A. D. (1997). Crater morphometry and modification in the sinus sabaeus and margaritifer sinus regions of Mars. *Journal of Geophysical Research: Planets*, *102*(E6), 13321–13340. doi: 10.1029/97JE01084

Day, M., Edgett, K. S., & Stumbaugh, D. (2019, December). Ancient stratigraphy preserving a wet-to-dry, fluvio-lacustrine to aeolian transition near barth crater, arabia terra, Mars. *Journal of Geophysical Research: Planets*, *124*(12), 3402–3421. doi: 10.1029/2019je006226

Dong, T. Y., & Goudge, T. A. (2022, 06). Quantitative relationships between river and channel-belt planform patterns. *Geology*, *50*(9), 1053–1057. doi: 10.1130/G49935.1

Dong, T. Y., Nittrouer, J. A., Czapiga, M. J., Ma, H., McElroy, B., Il'icheva, E., ... Parker, G. (2019, January). Roles of Bank Material in Setting Bankfull Hydraulic Geometry as Informed by the Selenga River Delta, Russia. *Water Resources Research*, *55*(1), 827–846. doi: 10.1029/2017WR021985

Dunne, K. B. J., & Jerolmack, D. J. (2018). Evidence of, and a proposed explanation for, bimodal transport states in alluvial rivers. *Earth Surface Dynamics*, *6*(3), 583–594. doi: 10.5194/esurf-6-583-2018

Dunne, K. B. J., & Jerolmack, D. J. (2020). What sets river width? *Science Advances*, *6*(41), eabc1505. doi: 10.1126/sciadv.abc1505

Edmonds, D. A., & Slingerland, R. L. (2010, February). Significant effect of sediment cohesion on delta morphology. *Nature Geoscience*, *3*(2), 105–109. doi: 10.1038/ngeo730

Edwards, M. B., & Eri, K. A. (1983). Paleochannel geometry and flow patterns determined from exhumed permian point bars in north-central texas. *SEPM Journal of Sedimentary Research*, *Vol. 53*. doi: 10.1306/212f835a-2b24-11d7-8648000102c1865d

Fassett, C. I. (2016). Analysis of impact crater populations and the geochronology of planetary surfaces in the inner solar system. *Journal of Geophysical Research: Planets*, *121*(10), 1900–1926. doi: 10.1002/2016JE005094

Fassett, C. I., & Head, J. W. (2008, May). The timing of Martian valley network activity: Constraints from buffered crater counting. *Icarus*, *195*(1), 61–89. doi: 10.1016/j.icarus.2007.12.009

Fassett, C. I., & Head III, J. W. (2005). Fluvial sedimentary deposits on Mars: Ancient deltas in a crater lake in the nili fossae region. *Geophysical Research Letters*, *32*(14). doi: 10.1029/2005GL023456

Forsberg-Taylor, N. K., Howard, A. D., & Craddock, R. A. (2004). Crater degradation in the Martian highlands: Morphometric analysis of the sinus sabaeus region and simulation modeling suggest fluvial processes. *Journal of Geophysical Research: Planets*, *109*(E5). doi: 10.1029/2004JE002242

Frazier, D. E. (1967). Recent deltaic deposits of the Mississippi River: their development and chronology. *Transactions of the Gulf Coast Association of Geological Societies*, *27*, 287–315.

Ganti, V., Straub, K. M., Foufoula-Georgiou, E., & Paola, C. (2011). Space-time dynamics of depositional systems: Experimental evidence and theoretical modeling of heavy-tailed statistics. *Journal of Geophysical Research: Earth Surface*, *116*(F2). doi: 10.1029/2010JF001893

Golombek, M., Robinson, K., McEwen, A., Bridges, N., Ivanov, B., Tornabene, L., & Sullivan, R. (2010). Constraints on ripple migration at meridiani planum from opportunity and hirise observations of fresh craters. *Journal of Geophysical Research: Planets*, *115*(E7). doi: 10

.1029/2010JE003628

Golombek, M. P., Grant, J. A., Crumpler, L. S., Greeley, R., Arvidson, R. E., Bell III, J. F., ... Squyres, S. W. (2006). Erosion rates at the Mars exploration rover landing sites and long-term climate change on Mars. *Journal of Geophysical Research: Planets*, *111*(E12). doi: 10.1029/2006JE002754

Golombek, M. P., Warner, N. H., Ganti, V., Lamb, M. P., Parker, T. J., Fergason, R. L., & Sullivan, R. (2014). Small crater modification on meridiani planum and implications for erosion rates and climate change on Mars. *Journal of Geophysical Research: Planets*, *119*(12), 2522–2547. doi: 10.1002/2014JE004658

Goudge, T. A., Mohrig, D., Cardenas, B. T., Hughes, C. M., & Fassett, C. I. (2018, February). Stratigraphy and paleohydrology of delta channel deposits, jezero crater, Mars. *Icarus*, *301*, 58–75. Retrieved from `https://doi.org/10.1016/j.icarus.2017.09.034` doi: 10.1016/j.icarus.2017.09.034

Grotzinger, J., Arvidson, R., Bell, J., Calvin, W., Clark, B., Fike, D., ... Watters, W. (2005). Stratigraphy and sedimentology of a dry to wet eolian depositional system, Burns formation, Meridiani Planum, Mars. *Earth and Planetary Science Letters*, *240*(1), 11–72. doi: 10.1016/j.epsl.2005.09.039

Grotzinger, J. P., Crisp, J., Vasavada, A. R., Anderson, R. C., Baker, C. J., Barry, R., ... Wiens, R. C. (2012-09). Mars Science Laboratory Mission and Science Investigation. *Space Science Reviews*, *170*(1-4), 5–56. doi: 10.1007/s11214-012-9892-2

Grotzinger, J. P., Gupta, S., Malin, M. C., Rubin, D. M., Schieber, J., Siebach, K., ... Wilson, S. A. (2015, October). Deposition, exhumation, and paleoclimate of an ancient lake deposit, gale crater, Mars. *Science*, *350*(6257). doi: 10.1126/science.aac7575

Hajek, E. A., & Edmonds, D. A. (2014, March). Is river avulsion style controlled by floodplain morphodynamics? *Geology*, *42*(3), 199–202. doi: 10.1130/G35045.1

Hajek, E. A., & Straub, K. M. (2017). Autogenic sedimentation in clastic stratigraphy. *Annual Review of Earth and Planetary Sciences*, *45*(1), 681-709. doi: 10.1146/annurev-earth-063016-015935

Hariharan, J., Passalacqua, P., Xu, Z., Michael, H. A., Steel, E., Chadwick, A., ... Moodie, A. J. (2022). Modeling the dynamic response of river deltas to sea-level rise acceleration. *Journal of Geophysical Research: Earth Surface*, *127*(9). doi: 10.1029/2022JF006762

Hariharan, J., Wright, K., Moodie, A., Tull, N., & Passalacqua, P. (2023). Impacts of human modifications on material transport in deltas. *Earth Surface Dynamics*, *11*(3), 405–427. doi: 10.5194/esurf-11-405-2023

Hariharan, J., Xu, Z., Michael, H. A., Paola, C., Steel, E., & Passalacqua, P. (2021, August). Linking the surface and subsurface in river deltas—part 1: Relating surface and subsurface geometries. *Water Resources Research*, *57*(8). doi: 10.1029/2020wr029282

Hartmann, W. K. (1966). Martian cratering. *Icarus*, *5*(1), 565–576. doi: 10.1016/0019-1035(66)90071-6

Hartmann, W. K. (1971). Martian cratering iii: Theory of crater obliteration. *Icarus*, *15*(3), 410–428. doi: 10.1016/0019-1035(71)90119-9

Hartmann, W. K., & Neukum, G. (2001). Cratering chronology and the evolution of Mars. *Space Science Reviews*, *96*(1/4), 165–194. doi: 10.1023/a:1011945222010

Hayden, A. T., Lamb, M. P., Fischer, W. W., Ewing, R. C., McElroy, B. J., & Williams, R. M. (2019). Formation of sinuous ridges by inversion of river-channel belts in utah, usa, with implications for Mars. *Icarus*, *332*, 92–110. doi: 10.1016/j.icarus.2019.04.019

Herkenhoff, K. E., & Plaut, J. J. (2000). Surface ages and resurfacing rates of the polar layered deposits on Mars. *Icarus*, *144*(2), 243–253. doi: 10.1006/icar.1999.6287

Hiesinger, H., Head III, J. W., Wolf, U., Jaumann, R., & Neukum, G. (2002). Lunar mare basalt flow units: Thicknesses determined from crater size-frequency distributions. *Geophysical Research Letters*, *29*(8), 89-1–89-4. doi: 10.1029/2002GL014847

Hoke, M. R. T., & Hynek, B. M. (2009, August). Roaming zones of precipitation on ancient Mars as recorded in valley networks. *Journal of Geophysical Research: Planets*, *114*(E8). doi: 10.1029/2008je003247

Howard, A. (2004). Simple non-fluvial models of planetary surface modification, with application to Mars. In *Lunar and planetary science conference* (p. 1054).

Howard, A. D. (2007). Simulating the development of Martian highland landscapes through the interaction of impact cratering, fluvial erosion, and variable hydrologic forcing. *Geomorphology*, *91*(3), 332–363. doi: 10.1016/j.geomorph.2007.04.017

Irwin, R. P., Lewis, K. W., Howard, A. D., & Grant, J. A. (2015, July). Paleohydrology of eberswalde crater, Mars. *Geomorphology*, *240*, 83–101. Retrieved from `https://doi.org/10.1016/j.geomorph.2014.10.012` doi: 10.1016/j.geomorph.2014.10.012

Irwin, R. P., Tanaka, K. L., & Robbins, S. J. (2013, February). Distribution of early, middle, and late noachian cratered surfaces in the Martian highlands: Implications for resurfacing events and processes. *Journal of Geophysical Research: Planets*, *118*(2), 278–291. doi: 10.1002/jgre.20053

Ivanov, B. A. (2001). Mars/moon cratering rate ratio estimates. *Space Science Reviews*, *96*(1/4), 87–104. doi: 10.1023/a:1011941121102

Jerolmack, D. J., & Paola, C. (2007, November). Complexity in a cellular model of river avulsion. *Geomorphology*, *91*(3-4), 259–270. doi: 10.1016/j.geomorph.2007.04.022

Jerolmack, D. J., & Sadler, P. (2007). Transience and persistence in the depositional record of continental margins. *Journal of Geophysical Research: Earth Surface*, *112*(F3). doi: 10.1029/2006JF000555

Kim, W., Petter, A., Straub, K., & Mohrig, D. (2014, August). Investigating the autogenic process response to allogenic forcing: experimental geomorphology and stratigraphy. In A. W. Martinius, R. Ravnås, J. A. Howell, R. J. Steel, & J. P. Wonham (Eds.), *From Depositional Systems to Sedimentary Successions on the Norwegian Continental Margin* (pp. 127–138). Chichester, UK: John Wiley & Sons, Ltd. doi: 10.1002/9781118920435.ch5

Kite, E. S. (2019, January). Geologic constraints on early Mars climate. *Space Science Reviews*, *215*(1). doi: 10.1007/s11214-018-0575-5

Kite, E. S., Lucas, A., & Fassett, C. I. (2013). Pacing early Mars river activity: Embedded craters in the aeolis dorsa region imply river activity spanned $\geq$(1–20)myr. *Icarus*, *225*(1), 850–855. doi: 10.1016/j.icarus.2013.03.029

Kite, E. S., Mischna, M. A., Fan, B., Morgan, A. M., Wilson, S. A., & Richardson, M. I. (2022, May). Changing spatial distribution of water flow charts major change in Mars's greenhouse effect. *Science Advances*, *8*(21). doi: 10.1126/sciadv.abo5894

Kite, E. S., Williams, J.-P., Lucas, A., & Aharonson, O. (2014, April). Low palaeopressure of the Martian atmosphere estimated from the size distribution of ancient craters. *Nature Geoscience*, *7*(5), 335–339. doi: 10.1038/ngeo2137

Lapôtre, M. G. A., & Ielpi, A. (2020). The pace of fluvial meanders on Mars and implications for the western delta deposits of jezero crater. *AGU Advances*, *1*(2). doi: 10.1029/2019AV000141

Lauzon, R., & Murray, A. B. (2018). Comparing the cohesive effects of mud and vegetation on delta evolution. *Geophysical Research Letters*, *45*(19), 10,437-10,445. doi: 10.1029/2018GL079405

Lauzon, R., Piliouras, A., & Rowland, J. C. (2019, June). Ice and permafrost effects on delta morphology and channel dynamics. *Geophysical Research Letters*. doi: 10.1029/2019GL082792

Leeder, M. (1978). A Quantitative Stratigraphic Model for Alluvium, with Special Reference to Channel Deposit Density and Interconnectedness. *Fluvial Sedimentology*, *Memoir 5*, 587–596.

Lewis, K. W., & Aharonson, O. (2014, June). Occurrence and origin of rhythmic sedimentary rocks on Mars. *Journal of Geophysical Research: Planets*, *119*(6), 1432–1457. doi: 10.1002/2013je004404

Liang, M., Geleynse, N., Edmonds, D. A., & Passalacqua, P. (2015b, January). A reduced-complexity model for river delta formation – Part 2: Assessment of the flow routing scheme. *Earth Surface Dynamics*, *3*(1), 87–104. doi: 10.5194/esurf-3-87-2015

Liang, M., Van Dyk, C., & Passalacqua, P. (2016, February). Quantifying the patterns and dynamics of river deltas under conditions of steady forcing and relative sea level rise: QUANTIFYING DELTA PATTERNS AND DYNAMICS. *Journal of Geophysical Research: Earth Surface*, *121*(2), 465–496. doi: 10.1002/2015JF003653

Liang, M., Voller, V. R., & Paola, C. (2015a, January). A reduced-complexity model for river delta formation – Part 1: Modeling deltas with channel dynamics. *Earth Surface Dynamics*, *3*(1), 67–86. doi: 10.5194/esurf-3-67-2015

Limaye, A. B. S., & Lamb, M. P. (2013). A vector-based method for bank-material tracking in coupled models of meandering and landscape evolution. *Journal of Geophysical Research: Earth Surface*, *118*(4), 2421–2437. doi: https://doi.org/10.1002/2013JF002854

Malin, M. C., & Edgett, K. S. (2000). Sedimentary rocks of early Mars. *Science*, *290*(5498), 1927–1937. doi: 10.1126/science.290.5498.1927

Mangold, N., Adeli, S., Conway, S., Ansan, V., & Langlais, B. (2012, April). A chronology of early Mars climatic evolution from impact crater degradation. *Journal of Geophysical Research: Planets*, *117*(E4). doi: 10.1029/2011je004005

Matsubara, Y., Howard, A. D., & Irwin, R. P. (2018, November). Constraints on the noachian paleoclimate of the Martian highlands from landscape evolution modeling. *Journal of Geophysical Research: Planets*, *123*(11), 2958–2979. doi: 10.1029/2018je005572

McEwen, A. S., Eliason, E. M., Bergstrom, J. W., Bridges, N. T., Hansen, C. J., Delamere, W. A., ... Weitz, C. M. (2007). Mars reconnaissance orbiter's high resolution imaging science experiment (hirise). *Journal of Geophysical Research: Planets*, *112*(E5). doi: 10.1029/2005JE002605

Melosh, H. J. (1989). *Impact cratering : a geologic process*. New York, NY: Oxford University Press.

Michael, G. (2013). Planetary surface dating from crater size–frequency distribution measurements: Multiple resurfacing episodes and differential isochron fitting. *Icarus*, *226*(1), 885–890. doi: 10.1016/j.icarus.2013.07.004

Michael, G., Kneissl, T., & Neesemann, A. (2016). Planetary surface dating from crater size-frequency distribution measurements: Poisson timing analysis. *Icarus*, *277*, 279–285. doi: 10.1016/j.icarus.2016.05.019

Milliken, R. E., Grotzinger, J. P., & Thomson, B. J. (2010). Paleoclimate of Mars as captured by the stratigraphic record in gale crater. *Geophysical Research Letters*, *37*(4). doi: 10.1029/2009GL041870

Minton, D. A., Richardson, J. E., & Fassett, C. I. (2015). Re-examining the main asteroid belt as the primary source of ancient lunar craters. *Icarus*, *247*, 172–190. doi: 10.1016/j.icarus.2014.10.018

Mohrig, D., Heller, P. L., Paola, C., & Lyons, W. J. (2000). Interpreting avulsion process from ancient alluvial sequences: Guadalope-Matarranya system (northern Spain) and Wasatch Formation (western Colorado). *Geological Society of America Bulletin*, *112*(12), 1787–1803.

Moodie, A. J., Hariharan, J., Barefoot, E., & Passalacqua, P. (2021). pyDeltaRCM: a flexible numerical delta model. *Journal of Open Source Software*. doi: 10.21105/joss.03398

Moodie, A. J., Nittrouer, J. A., Ma, H., Carlson, B. N., Chadwick, A. J., Lamb, M. P., & Parker, G. (2019). Modeling deltaic lobe-building cycles and channel avulsions for the yellow river delta, china. *Journal of Geophysical Research: Earth Surface*, *124*(11), 2438–2462. doi: 10.1029/2019JF005220

Moodie, A. J., & Passalacqua, P. (2021). When does faulting-induced subsidence drive distributary network reorganization? *Geophysical Research Letters*, *48*(22). doi: 10.1029/2021GL095053

Neukum, G., & Horn, P. (1976). Effects of lava flows on lunar crater populations. *The Moon*, *15*(3-4), 205–222. doi: 10.1007/bf00562238

Öpik, E. J. (1966). The Martian surface. *Science*, *153*(3733), 255–265. doi: 10.1126/science.153.3733.255

Parker, G. (2004, November). *E-book: 1D sediment transport morphodynamics with applications to rivers and turbidity currents.* E-book. (Available at: http://hydrolab.illinois.edu/people/parkerg/morphodynamics_e-book.htm)

Parker, G., Paola, C., Whipple, K. X., Mohrig, D., Toro-Escobar, C. M., Halverson, M., & Skoglund, T. W. (1998, October). Alluvial Fans Formed by Channelized Fluvial and Sheet Flow. II: Application. *Journal of Hydraulic Engineering*, *124*(10), 996–1004. doi: 10.1061/(ASCE)0733-9429(1998)124:10(996)

Pike, R. J. (1977, January). Size-dependence in the shape of fresh impact craters on the moon. In D. J. Roddy, R. O. Pepin, & R. B. Merrill (Eds.), *Impact and explosion cratering: Planetary and terrestrial implications* (pp. 489–509).

Piliouras, A., Lauzon, R., & Rowland, J. C. (2021). Unraveling the combined effects of ice and permafrost on arctic delta morphodynamics. *Journal of Geophysical Research: Earth Surface*, *126*(4). doi: 10.1029/2020JF005706

Popova, O., Nemtchinov, I., & Hartmann, W. K. (2003, June). Bolides in the present and past Martian atmosphere and effects on cratering processes. *Meteoritics & Planetary Science*, *38*(6), 905–925. doi: 10.1111/j.1945-5100.2003.tb00287.x

Reitz, M. D., & Jerolmack, D. J. (2012, May). Experimental alluvial fan evolution: Channel dynamics, slope controls, and shoreline growth. *Journal of Geophysical Research*, *117*(F2). doi: 10.1029/2011JF002261

Reitz, M. D., Jerolmack, D. J., & Swenson, J. B. (2010, March). Flooding and flow path selection on alluvial fans and deltas: FLOW PATH SELECTION ON ALLUVIAL FANS. *Geophysical Research Letters*, *37*(6), n/a–n/a. doi: 10.1029/2009GL041985

Richardson, J. E. (2009). Cratering saturation and equilibrium: A new model looks at an old problem. *Icarus*, *204*(2), 697–715. doi: 10.1016/j.icarus.2009.07.029

Richardson, J. E., Melosh, H. J., & Greenberg, R. (2004). Impact-induced seismic activity on asteroid 433 eros: A surface modification process. *Science*, *306*(5701), 1526–1529. doi: 10.1126/science.1104731

Richardson, J. E., Melosh, H. J., Greenberg, R. J., & O'Brien, D. P. (2005). The global effects of impact-induced seismic activity on fractured asteroid surface morphology. *Icarus*, *179*(2), 325–349. doi: 10.1016/j.icarus.2005.07.005

Robbins, S. J., & Hynek, B. M. (2012). A new global database of Mars impact craters $\geq$1 km: 2. global crater properties and regional variations of the simple-to-complex transition diameter. *Journal of Geophysical Research: Planets*, *117*(E6). doi: 10.1029/2011JE003967

Ross, H. P. (1968). A simplified mathematical model for lunar crater erosion. *Journal of Geophysical Research (1896-1977)*, *73*(4), 1343–1354. doi: 10.1029/JB073i004p01343

Russ, J. C. (1986). *Practical stereology*. Springer US. doi: 10.1007/978-1-4899-3533-5

Sadler, P. M. (1981). Sediment accumulation rates and the completeness of stratigraphic sections. *The Journal of Geology*, *89*(5), 569–584. doi: 10.1086/628623

Schultz, P. H., & Gault, D. E. (1975, January). Seismically induced modification of lunar surface features. *Lunar and Planetary Science Conference Proceedings*, *3*, 2845–2862.

Schumer, R., Jerolmack, D., & McElroy, B. (2011). The stratigraphic filter and bias in measurement of geologic rates. *Geophysical Research Letters*, *38*(11). doi: 10.1029/2011GL047118

Schumm, S. A. (1985). Patterns of alluvial rivers. *Annual Review of Earth and Planetary Sciences*, *13*(1), 5–27. doi: 10.1146/annurev.ea.13.050185.000253

Shannon, C. (1949). Communication in the Presence of Noise. *Proceedings of the IRE*, *37*(1), 10–21. doi: 10.1109/JRPROC.1949.232969

Slingerland, R., & Smith, N. D. (2004, May). RIVER AVULSIONS AND THEIR DEPOSITS. *Annual Review of Earth and Planetary Sciences*, *32*(1), 257–285. doi: 10.1146/annurev.earth.32.101802.120201

Smith, M. R., Gillespie, A. R., & Montgomery, D. R. (2008). Effect of obliteration on crater-count chronologies for Martian surfaces. *Geophysical Research Letters*, *35*(10). doi: 10.1029/2008GL033538

Smith, N. D., Cross, T. A., Dufficy, J. P., & Clough, S. R. (1989, February). Anatomy of an avulsion. *Sedimentology*, *36*(1), 1–23. doi: 10.1111/j.1365-3091.1989.tb00817.x

Soderblom, L. A. (1970). A model for small-impact erosion applied to the lunar surface. *Journal of Geophysical Research (1896-1977)*, *75*(14), 2655–2661. doi: 10.1029/JB075i014p02655

Stack-Morgan, K. M., Gupta, S., Tebolt, M., Caravaca, G., Ives, L. R., Russell, P., … Williams, R. M. (2023). Sedimentology and stratigraphy of the lower delta sequence, jezero crater, Mars. The Woodlands, TX, USA.

Straub, K. M., Duller, R. A., Foreman, B. Z., & Hajek, E. A. (2020). Buffered, incomplete, and shredded: The challenges of reading an imperfect stratigraphic record. *Journal of Geophysical Research: Earth Surface*, *125*(3). doi: 10.1029/2019JF005079

Straub, K. M., & Esposito, C. R. (2013). Influence of water and sediment supply on the stratigraphic record of alluvial fans and deltas: Process controls on stratigraphic completeness. *Journal of Geophysical Research: Earth Surface*, *118*(2), 625-637. doi: 10.1002/jgrf.20061

Straub, K. M., Li, Q., & Benson, W. M. (2015). Influence of sediment cohesion on deltaic shoreline dynamics and bulk sediment retention: A laboratory study. *Geophysical Research Letters*, *42*(22), 9808–9815. doi: 10.1002/2015GL066131

Straub, K. M., Paola, C., Mohrig, D., Wolinsky, M. A., & George, T. (2009, 09). Compensational Stacking of Channelized Sedimentary Deposits. *Journal of Sedimentary Research*, *79*(9), 673-688. doi: 10.2110/jsr.2009.070

Stucky de Quay, G., Goudge, T. A., Kite, E. S., Fassett, C. I., & Guzewich, S. D. (2021, August). Limits on runoff episode duration for early Mars: Integrating lake hydrology and climate models. *Geophysical Research Letters*, *48*(15). doi: 10.1029/2021gl093523

Tejedor, A., Schwenk, J., Kleinhans, M., Limaye, A. B., Vulis, L., Carling, P., … Foufoula-Georgiou, E. (2022, August). The entropic braiding index (ebi): A robust metric to account for the diversity of channel scales in multi-thread rivers. *Geophysical Research Letters*, *49*(16). doi: 10.1029/2022gl099681

Trampush, S. M., Huzurbazar, S., & McElroy, B. (2014). Empirical assessment of theory for bankfull characteristics of alluvial channels. *Water Resources Research*, *50*(12), 9211-9220. doi: 10.1002/2014WR015597

Vasavada, A. R. (2022). Mission Overview and Scientific Contributions from the Mars Science Laboratory Curiosity Rover After Eight Years of Surface Operations. *Space Science Reviews*,

218(3), 14. doi: 10.1007/s11214-022-00882-7

Wang, Y., Straub, K. M., & Hajek, E. A. (2011). Scale-dependent compensational stacking: An estimate of autogenic time scales in channelized sedimentary deposits. *Geology*, *39*(9), 811–814. doi: 10.1130/G32068.1

Warren, A. O., Kite, E. S., Williams, J.-P., & Horgan, B. (2019). Through the thick and thin: New constraints on Mars paleopressure history 3.8–4 ga from small exhumed craters. *Journal of Geophysical Research: Planets*, *124*(11), 2793–2818. doi: 10.1029/2019JE006178

Wells, N. A., & Dorr, J. A. (1987). Shifting of the Kosi River, northern India. *Geology*, *15*(3), 204. doi: 10.1130/0091-7613(1987)15$⟨$204:SOTKRN$⟩$2.0.CO;2

Wickert, A. D., Martin, J. M., Tal, M., Kim, W., Sheets, B., & Paola, C. (2013, June). River channel lateral mobility: metrics, time scales, and controls: RIVER CHANNEL LATERAL MOBILITY. *Journal of Geophysical Research: Earth Surface*, *118*(2), 396–412. doi: 10.1029/2012JF002386

Williams, J.-P., Pathare, A. V., & Aharonson, O. (2014). The production of small primary craters on Mars and the moon. *Icarus*, *235*, 23–36. doi: 10.1016/j.icarus.2014.03.011

Williams, J.-P., van der Bogert, C. H., Pathare, A. V., Michael, G. G., Kirchoff, M. R., & Hiesinger, H. (2018). Dating very young planetary surfaces from crater statistics: A review of issues and challenges. *Meteoritics & Planetary Science*, *53*(4), 554–582. doi: 10.1111/maps.12924

Wolman, M. G., & Miller, J. P. (1960, January). Magnitude and Frequency of Forces in Geomorphic Processes. *The Journal of Geology*, *68*(1), 54–74. doi: 10.1086/626637

Woronow, A. (1977). Crater saturation and equilibrium: A monte carlo simulation. *Journal of Geophysical Research (1896-1977)*, *82*(17), 2447–2456. doi: 10.1029/JB082i017p02447

Woronow, A. (1978). A general cratering-history model and its implications for the lunar highlands. *Icarus*, *34*(1), 76–88. doi: 10.1016/0019-1035(78)90127-6

Wright, K., Hariharan, J., Passalacqua, P., Salter, G., & Lamb, M. P. (2022). From grains to plastics: Modeling nourishment patterns and hydraulic sorting of fluvially transported materials in deltas. *Journal of Geophysical Research: Earth Surface*, *127*(11), e2022JF006769. doi: 10.1029/2022JF006769

Yielding, G., Needham, T., & Jones, H. (1996). Sampling of fault populations using sub-surface data: a review. *Journal of Structural Geology*, *18*(2), 135–146. doi: 10.1016/S0191-8141(96)80039-3